D. Qi, A. J. Majda *Res Math Sci* (2020) 7:22
https://doi.org/10.1007/s40687-020-00219-2

Research in the Mathematical Sciences

RESEARCH

Nonlinear interaction and turbulence transition in the limiting regimes of plasma edge turbulence

Di Qi and Andrew J. Majda

*Correspondence:
qidi@cims.nyu.edu
Department of Mathematics and Center for Atmosphere and Ocean Science, Courant Institute of Mathematical Sciences, New York University, New York, NY 10012, USA

Abstract

We study the nonlinear coupling mechanism and turbulent transition in magnetically confined plasma flows based on two representative limiting regime dynamics. The two-field flux-balanced Hasegawa–Wakatani (BHW) model is taken as a simplified approximation to the key physical processes in the energy-conserving nonlinear plasma flows. The limiting regimes separate the effects of finite non-adiabatic resistivity and extreme non-normal dynamics to enable a more detailed investigation on each individual aspect with the help of various mathematical tools. We adopt the strategy from the selective decay theory used for the simpler one-field system to develop new crucial *a priori* estimations in the two-field model framework. The competing effects from model dissipation, finite particle resistivity, as well as the nonlinear interaction with a zonal mean state to induce dual direction energy transports are characterized from the systematic analysis. Non-normal dynamics with aligned eigendirections is also shown to go through a sharp transition from turbulence to regularized zonal flows. The diverse phenomena implied from the limiting regime analysis are further confirmed from direct numerical simulations of the BHW model.

1 Introduction

Nonlinear interactions between the turbulent non-zonal waves and the self-organized zonal flow play a critical role in many observed phenomena from natural and experimental systems [9,10,13,17,19]. One example of particular interest comes from the generation and development of turbulent transport in the edge regime of toroidal magnetically confined plasmas [2,3,5,8,14]. The nonlinear exchange of energy among wide scales can be developed from secondary instability and lead to the emergence of persistent large-scale zonal structures from the turbulent transition [21,22]. This phenomenon is also related with the Dimits shift [4,25,28] which refers to a nonlinear upshift in the amplitude of the turbulent flow transport. To understand the fundamental physics in such complex nonlinear systems is crucial with significant practical importance such as the achievement of controlled fusion; thus, it still attracts extensive researches in theoretical and numerical exploration of the mechanisms in representative fusion plasma phenomena [1,11,12,26].

The use of simplified model framework plays an important role in identifying the key physical constituents for the analysis of plasma confinement and anomalous transport. Among them, the one-field Hasegawa–Mima (HM) [2,6] and the two-field Hasegawa–Wakatani (HW) [7,18,27] models provide simplified formulations for the drift wave–zonal flow interaction mechanism to qualitatively capture the energy-conserving nonlinear processes in plasma flows. In a recent development, a flux-balanced Hasegawa–Wakatani (BHW) model is proposed [14,24] to introduce an improved balanced treatment in the parallel electron responses on magnetic flux surfaces, compared with the previous modified Hasegawa–Wakatani (MHW) formulation [2,7]. The BHW model with generic drift instability and balanced particle response provides a more feasible formulation where the most essential physical processes are identified [14,20]. Besides, it is shown that this model is able to recover the representative nonlinear Dimits shift and the intermittent avalanche-like bursts [23,25] that are of particular interest in more complicated model simulations.

In this paper, we investigate the complex turbulent structures in magnetically confined plasma edge flows by inspecting the typical limiting dynamical regimes. The complicated plasma equations combining the interplay of various linear and nonlinear interactions usually make it impossible to carry out direct theoretical analysis for the basic features. The one-field HM model offers a clean setup with analytical tractability for the application of mathematical theories such as the selective decay principle and nonlinear secondary instability [21,22]. On the other hand, the HM model is often insufficient by only including the most basic adiabatic dynamics with zero particle resistivity and no instability. To introduce the effects from the non-adiabatic electron response α and the unstable drift waves from background ion density gradient κ, we need to move to the next level two-field BHW model containing richer phenomena from a larger group of coupled components. Especially, important processes to be investigated include the excitation of linear drift wave instability; the coupling between the characterizing stable and unstable subdirections; and the non-normal coupling dynamics in relation to the two major model parameters α, κ.

The typical features in the plasma system such as the statistical transition from strong turbulent particle transport to pure zonal flow regime are usually a result from a combination of several interacting effects from the model. In describing the complicated mechanism including multiple coupled processes, a desirable strategy is to separate each individual component to analyze them in a simpler setup and then to consider their combined contributions. In the two-field BHW model case, the situation becomes more challenging with multiple factors acting in opposite directions to create the final turbulent solutions. Selective decay principle [15,17] is one effective strategy for showing the accumulation of energy in different scales. The theory framework is successfully applied to predict the emergence of a purely zonal state in the one-field HM model subject to generalized dissipations [21,22]. However, we can no longer find the similar clean convergence result for the two-field BHW model as in the one-field HM case. Instead, we adopt the general strategy to separate the effect from different processes and take a more heuristic approach for the analysis of each individual contribution. A sketch of the mathematical theory is first provided to quantify the effect from each model component. New crucial *a priori* estimations are then developed based on the mathematical theory. To support the theoretical discoveries, extensive numerical simulations are carried out to illustrate the predicted features.

In particular here, we aim to address the following major issues in this paper according to the BHW model:

(i) Linear mode interactions from model parameters κ, α: the linear stability analysis decomposes the state space into the unstable and stable subspaces by the eigenvalue decomposition of the linearized operator L for each wavenumber. The model parameters κ, α determine the growth/damping rate along the unstable/stable subdirections and lead to a transition from normal subdirections to fully non-normal dynamics.

(ii) Non-normal dynamics due to the parameter ratio $r = \frac{\kappa}{\alpha}$: It is found that strong non-normal dynamics can be generated for the two eigendirections as $r \to \infty$. The two eigenvectors can be determined only dependent on the parameter ratio $r = \frac{\kappa}{\alpha}$. Non-normal interactions introduce additional complexity into the coupling between the two characterizing eigenmodes.

(iii) Nonlinear interaction between the two eigendirections based on the adiabaticity α: By setting the background density gradient parameter $\kappa = 0$, we are able to study the interaction between the two eigendirections due to varying α without linear instability and non-normal dynamics. This limiting case considers the redistribution (both downscale and upscale) of the excited energy purely due to the effect from the resistivity parameter α. And the finite resistivity α is shown to have the reversed selective decay driving the energy in the opposite direction to the selective decay from the dissipation of fluctuation modes.

(iv) Extreme non-normal dynamics based on background density gradient κ: By setting the parameter $\alpha = 0$, we reach the other limiting regime where the two eigendirections are aligned with each other. The density field is comparable to a passive tracer field with zonal mean gradient. In this case, we are able to investigate the effect of strong non-normal coupling between eigenmodes, and the particle flux transport with and without the contribution from a dominant zonal flow through direct numerical simulations.

In the rest part of the paper, a general description of the model formulation and key properties of linear instability and conserved quantities is first provided in Sect. 2. Then, the two major limiting regimes of interest are discussed. Section 3 studies the nonlinear energy transfer mechanisms due to different effects in the limiting regime $\kappa = 0$ using the selective decay theory. And the other extreme limiting regime with $\alpha = 0$ is studied in Sect. 4 concentrating on the non-normal dynamics and the transition from turbulence to regularized zonal flows. The concluding discussion is provided in Sect. 5.

2 Separating coupling effects in the two-field model for plasma edge turbulence

The *flux-balanced Hasegawa–Wakatani* (BHW) equations model the coupling between drift wave modes and zonal state with balanced particle responses on the embedded magnetic surfaces [14,24]. The system includes both drift waves from background ion density gradient and non-adiabatic electron responses. It is formulated based on the flux-balanced *potential vorticity* $q = \nabla^2\varphi - \tilde{n}$ and the *density fluctuation* n in the following

two-dimensional equations

$$\frac{\partial q}{\partial t} + \nabla^{\perp}\varphi \cdot \nabla q - \kappa \frac{\partial \varphi}{\partial y} = \mu \Delta q, \tag{1a}$$

$$\frac{\partial n}{\partial t} + \nabla^{\perp}\varphi \cdot \nabla n + \kappa \frac{\partial \varphi}{\partial y} = \alpha \left(\tilde{\varphi} - \tilde{n}\right) + \mu \Delta n, \tag{1b}$$

where φ is the electrostatic potential, n is the density fluctuation from the prescribed background density $n_0(x)$, and $\mathbf{u}_E \equiv \nabla^{\perp}\varphi = \left(-\partial_y\varphi, \partial_x\varphi\right)$ is the $\mathbf{E} \times \mathbf{B}$ velocity field. The solutions are usually defined on a doubly periodic geometry for the sake of simplicity, while it can be easily generalized to other geometry such as a channel domain [23,25].

The model dynamical structure in (1) is determined by two major control parameters, that is, κ and α. The constant background density gradient $\kappa = -\nabla \ln n_0$ is defined by the exponential background density profile near the boundary $n_0(x) \sim \exp(-\kappa x)$. The non-adiabatic resistivity parameter (adiabaticity) α for parallel electron motions is inversely related to the particle resistivity. It determines the degree to which electrons can move rapidly along the magnetic field lines [7,8]. On the right hand sides of the Eq. (1), another effect of collisional ion viscosity is modeled as a homogeneous dissipation approximated by the Laplace operator with strength μ uniformly on both potential vorticity and particle density field [16].

For convenience in analysis of the drift wave–zonal flow interactions, the physical quantities for φ and n are usually decomposed into zonally averaged mean states $\bar{\varphi}$, $\bar{n}$ and their fluctuations $\tilde{\varphi}$, $\tilde{n}$ about the zonal mean, that is,

$$\varphi = \bar{\varphi} + \tilde{\varphi}, \ n = \bar{n} + \tilde{n}, \quad \overline{f}(x) = L_y^{-1} \int_0^{L_y} f(x, y)\, \mathrm{d}y. \tag{2}$$

The important modification in the BHW model comes from the removed of the poloidally averaged density $\bar{n}$ along y-direction from the potential vorticity $q = \nabla^2\varphi - \tilde{n}$. In contrast, the original and modified Hasegawa–Wakatani (MHW) models introduced in [2,27] use the 'unbalanced' potential density $q = \nabla^2\varphi - n$ without removing the mean state $\overline{n}$ in the potential vorticity, leading to problems with the convergence at the adiabatic limit $\alpha \to \infty$ [21,22,24].

The BHW model offers a more realistic formulation with many desirable properties [20–23]. Especially, it is shown from rigorous proof and numerical confirmation [14,24] that at the adiabatic limit, $\alpha \to \infty$, the BHW model converges to the following one-state equation about the potential vorticity

$$\frac{\partial q}{\partial t} + \nabla^{\perp}\varphi \cdot \nabla q - \kappa \frac{\partial \varphi}{\partial y} = \mu \Delta q, \quad q = \nabla^2\varphi - \tilde{\varphi}, \tag{3}$$

which is called the *modified Hasegawa–Mima* (MHM) model [2,6]. Notice again the modification by removing zonal state in $\tilde{\varphi}$ in the definition of potential vorticity q in the above Eq. (3). On the other hand, the MHW model shows performance significantly different from the converging BHM model as $\alpha \to \infty$ [23,24].

2.1 Linear and nonlinear coupling effects in the two-field model

The fluctuation states $(\tilde{q}, \tilde{n})$ in the non-zonal modes $k_y \neq 0$ can be Galerkin projected to the spectral domain with Fourier modes due to the doubly periodic boundary condition

$$\tilde{q} = \sum_{\mathbf{k}} \hat{q}_{\mathbf{k}} e^{i(\mathbf{k}\cdot\mathbf{x}-\omega_{\mathbf{k}}t)}, \ \tilde{n} = \sum_{\mathbf{k}} \hat{n}_{\mathbf{k}} e^{i(\mathbf{k}\cdot\mathbf{x}-\omega_{\mathbf{k}}t)}; \tag{4}$$

and the corresponding potential function $\tilde{\varphi}$ is recovered from the fluctuation state relation $\tilde{q} = \nabla^2\tilde{\varphi} - \tilde{n}$

$$\tilde{\varphi} = \sum_{\mathbf{k}} \hat{\varphi}_{\mathbf{k}} e^{i(\mathbf{k}\cdot\mathbf{x}-\omega_{\mathbf{k}}t)} = -\sum_{\mathbf{k}} k^{-2} \left(\hat{q}_{\mathbf{k}} + \hat{n}_{\mathbf{k}}\right) e^{i(\mathbf{k}\cdot\mathbf{x}-\omega_{\mathbf{k}}t)}.$$

Above $\omega_{\mathbf{k}} = \omega(\mathbf{k})$ is the wave frequency for each corresponding wavenumber and $k = |\mathbf{k}|$ is the absolute length of the two-dimensional wavenumber. In the analysis of typical model properties, we can summarize the Eq. (1) in a general form. The model can be expressed by the Fourier coefficients $\mathbf{u}_{\mathbf{k}} = (\hat{q}_{\mathbf{k}}, \hat{n}_{\mathbf{k}})^T$ as 2×2 subsystems for each wavenumber $\mathbf{k}$. Substituting the above spectral expressions (4) into the original Eq. (1), we rewrite the original equations in the following form:

$$\frac{\mathrm{d}\mathbf{u}_{\mathbf{k}}}{\mathrm{d}t} + N_{\mathbf{k}}(\mathbf{u}) = \alpha L_{\mathbf{k}}\mathbf{u}_{\mathbf{k}} - D_{\mathbf{k}}\mathbf{u}_{\mathbf{k}}. \tag{5}$$

Above L and D are the linear operators for the skew symmetric dispersion and negative definite dissipation effects. The linear matrix L is only dependent on the parameter ratio $r = \kappa/\alpha$ so that

$$L_{\mathbf{k}} = -\begin{bmatrix} 0 & 0 \\ k^{-2} & 1+k^{-2} \end{bmatrix} + irk_y k^{-2} \begin{bmatrix} -1 & -1 \\ 1 & 1 \end{bmatrix}, \quad r = \frac{\kappa}{\alpha}.$$

Homogeneous damping is represented by the diagonal operator $D_{\mathbf{k}} = -\mu k^2 I$. The nonlinear operator N contains all the nonlinear coupling due to the flow advection term

$$N_{\mathbf{k}} = \begin{bmatrix} \left(\nabla^{\perp}\varphi \cdot \nabla q\right)_k \\ \left(\nabla^{\perp}\varphi \cdot \nabla n\right)_k \end{bmatrix} = \begin{bmatrix} \sum_{\mathbf{m}+\mathbf{n}=\mathbf{k}} \frac{\mathbf{m}^{\perp}\cdot\mathbf{n}}{m^2}\left(\hat{q}_{\mathbf{m}} + \hat{n}_{\mathbf{m}}\right)\hat{q}_{\mathbf{n}} \\ \sum_{\mathbf{m}+\mathbf{n}=\mathbf{k}} \frac{\mathbf{m}^{\perp}\cdot\mathbf{n}}{m^2}\left(\hat{q}_{\mathbf{m}} + \hat{n}_{\mathbf{m}}\right)\hat{n}_{\mathbf{n}} \end{bmatrix},$$

where the effects from different scales are intertwined from the nonlinear interaction. It can be seen next that the nonlinear operator N will not change the total energy and enstropy of the system [14]. The advantage of considering the above 2×2 subsystems (5) is that we can diagonalize the linear operators. Then, by the eigenvalue decomposition of the linear matrix, we can find the transform matrix P for the eigenvectors and the diagonalized matrix Λ for the eigenvalues

$$PL = \Lambda P, \quad \mathbf{v} = P\mathbf{u}.$$

The original system (5) can be transformed into the diagonalized system about $\mathbf{v} = (v_1, v_2)^T$

$$\frac{\mathrm{d}\mathbf{v}}{\mathrm{d}t} = -\Lambda\mathbf{v} - PN\left(P^{-1}\mathbf{v}\right). \tag{6}$$

Above, v_1 becomes the unstable eigenmode and v_2 is the stable eigenmode from the linear stability analysis. $\Lambda = \mathrm{diag}(\lambda_1, \lambda_2)$ is the diagonal matrix for the two eigenvalues. The two stable and unstable directions as well as different scales are coupled through the nonlinear term N.

2.1.1 Stable and unstable subdirections in the BHW model

Linear stability analysis of the BHW model (5) offers the driving mechanism for the generation of non-zonal fluctuations in the starting transient state. This linear instability generated from the drift wave resistivity leads to the excitation of non-zonal drift wave modes from the initial state with only small perturbations. The linear operator decomposes the system into the stable and unstable subspaces (6) with exponential growth and damping along the corresponding eigendirections. The explicit formulas for the characteristic stable and unstable subdirections of the BHW system can be then computed.

Drift wave instability is due to the non-adiabatic electron response with finite $\alpha \neq 0$. Neglecting the nonlinear coupling terms N, the linearized Eq. (5) for a single non-zonal wavenumber $k_y \neq 0$ yield

$$\begin{aligned} -i\omega\hat{q} - i\kappa k_y\hat{\varphi} &= -\mu k^2\hat{q}, \\ -i\omega\hat{n} + i\kappa k_y\hat{\varphi} &= \alpha\left(\hat{\varphi} - \hat{n}\right) - \mu k^2\hat{n}. \end{aligned} \tag{7}$$

The above system can be decoupled into independent subsystems (6) for each single wavenumber $\mathbf{k}$ since we do not include the nonlinear terms in the linearized system. It can be viewed as the dominant dynamics in the starting transient state when the state values are small and nonlinear interactions have not taken the major effect. The linearized coefficients $(\hat{q}, \hat{n})$ then form the 2×2 subsystem for each wavenumber. We organize the linear coupling terms including the drift instability on the left hand side of (7) and the stabilizing dissipations on the right hand side. In fact, in the homogeneous damping case, the dissipation operator on the right hand side of (7) becomes diagonal. It can be eliminated by introducing the additional damping effects into the single wavenumber modes by

$$\tilde{q} = \hat{q}e^{i\mathbf{k}\cdot\mathbf{x}}e^{-i\varpi t}e^{\sigma t - \mu k^2 t}, \quad \tilde{n} = \hat{n}e^{i\mathbf{k}\cdot\mathbf{x}}e^{-i\varpi t}e^{\sigma t - \mu k^2 t},$$

where we decompose the frequency ω into the real and imaginary parts. The two branches of the eigenvalues $\omega^+ = \varpi + i\sigma^+$ and $\omega^- = -\varpi + i\sigma^-$ can be computed explicitly [20] as

$$\begin{aligned} \varpi_{\mathbf{k}} &= \frac{\operatorname{sgn}\left(k_y\right)\alpha}{2\sqrt{2}}\left(1 + k^{-2}\right)\left(\sqrt{1 + 16\gamma^2} - 1\right)^{\frac{1}{2}}, \\ \sigma^+_{\mathbf{k}} &= \frac{\alpha}{2}\left(1 + k^{-2}\right)\left[\frac{1}{\sqrt{2}}\left(\sqrt{1 + 16\gamma^2} + 1\right)^{\frac{1}{2}} - 1\right], \\ \sigma^-_{\mathbf{k}} &= -\frac{\alpha}{2}\left(1 + k^{-2}\right)\left[\frac{1}{\sqrt{2}}\left(\sqrt{1 + 16\gamma^2} + 1\right)^{\frac{1}{2}} + 1\right], \end{aligned} \tag{8}$$

with the only parameter dependence on the ratio $\gamma = \frac{\kappa}{\alpha}\frac{k_y k^2}{\left(1+k^2\right)^2}$. The detailed discussion for the two branches of explicit solutions of the dispersion relation can be found in Section III of [20].

The two sets of eigenvalues $\omega^\pm = \pm\varpi + i\sigma^\pm$ also give the two branches of eigendirections for the two state pair $\left(\hat{q}^\pm, \hat{n}^\pm\right)$ and the corresponding potential function $\hat{\varphi}^\pm$ as

$$\hat{n}^\pm = \left(\kappa^{-1}k_y^{-1}k^2\omega^\pm - 1\right)\hat{q}^\pm, \quad \hat{\varphi}^\pm = -\kappa^{-1}k_y^{-1}\omega^\pm\hat{q}^\pm. \tag{9}$$

The unstable direction with $\sigma^+ > 0$ implies exponential growth along this eigendirection from the linear drift instability; the stable direction $\sigma^- < 0$ implies exponential decay along the eigendirection. The two eigenvectors $\left(\hat{q}^{\pm}, \hat{n}^{\pm}\right)$ of unstable and stable modes can be found explicitly from the previous expression (9) together with the explicit formulas (8) as

$$\begin{aligned}
\text{unstable direction: } \mathbf{u_k}^+ &= \left(\hat{q}_{\mathbf{k}}^+, \hat{n}_{\mathbf{k}}^+\right) \\
&= C_+ \left(2\sqrt{2}\gamma\left(1+k^2\right), -\left(\sqrt{1+16\gamma^2}-1\right)^{\frac{1}{2}}\right. \\
&\quad \left. +i\left[\left(\sqrt{1+16\gamma^2}+1\right)^{\frac{1}{2}} - \sqrt{2}\right]\right)^T; \\
\text{stable direction: } \mathbf{u_k}^- &= \left(\hat{q}_{\mathbf{k}}^-, \hat{n}_{\mathbf{k}}^-\right) \\
&= C_- \left(2\sqrt{2}\gamma\left(1+k^2\right), \quad \left(\sqrt{1+16\gamma^2}-1\right)^{\frac{1}{2}}\right. \\
&\quad \left. -i\left[\left(\sqrt{1+16\gamma^2}+1\right)^{\frac{1}{2}} + \sqrt{2}\right]\right)^T,
\end{aligned} \tag{10}$$

where C_+, C_- are factors to normalize the vectors to unit length.

2.1.2 Angles between the two eigendirections for the non-dissipative drift waves

The non-normal dynamics considers the alignment of the two above eigenvectors. Non-normal structures become important when the background density is nonzero $\kappa \neq 0$. The eigendirections in (10) as a function of $\gamma = r\frac{k_y k^2}{\left(1+k^2\right)^2}$ also only depend on the two parameter ratio $r = \frac{\kappa}{\alpha}$. Thus, they gain the self-similarity based on the value of $\frac{\kappa}{\alpha}$. As the ratio approaches the zero limit $r \to 0$, the two eigenvectors tend to become orthogonal with each other, while at the infinity limit $r \to \infty$, the modes (especially the pure drift mode $k_x = 0$) become aligned along the same direction.

To check the alignment between the two characteristic eigendirections in (10), we define the *angle* $\theta_{\mathbf{k}}(r)$ between the two vectors $\left(\mathbf{u_k}^+, \mathbf{u_k}^-\right)$ by the complex inner product

$$\cos\theta_{\mathbf{k}}(r) = \frac{\mathfrak{Re}\left\langle \mathbf{u_k}^+, \mathbf{u_k}^- \right\rangle}{\left\| \mathbf{u_k}^+ \right\| \left\| \mathbf{u_k}^- \right\|}, \tag{11}$$

where $\langle a, b\rangle = \sum a_i b_i^*$ and $\mathbf{u_k}^+ = \left(\hat{q}_{\mathbf{k}}^+, \hat{n}_{\mathbf{k}}^+\right)^T$, $\mathbf{u_k}^- = \left(\hat{q}_{\mathbf{k}}^-, \hat{n}_{\mathbf{k}}^-\right)^T$. The angle $\theta_{\mathbf{k}}(r)$ characterizes the alignment of two eigenvectors for each wavenumber $\mathbf{k}$ and is only dependent on the parameter ratio $r = \kappa/\alpha$. Along the zonal direction $k_y = 0$, obviously the two eigenvectors become orthogonal to each other. As an illustration of the linear instability and non-normal structure in the eigenmodes dependent on the parameters, Fig. 1 plots the angles (11) between the two eigenvectors in the spectral domain among different wavenumbers $\mathbf{k} = (k_x, k_y)$, and the changes in the most non-normal wavenumber as a function of the parameter ratio $r = \frac{\kappa}{\alpha}$. The first row shows the angles in degree for each wavenumber in the two-dimensional spectral domain. With small values of the ratio r, the two modes are mostly orthogonal among all the wavenumbers. As the value of the ratio r increases, the non-normality grows larger. The most non-normal modes are along the line of pure drift wave modes $k_x = 0$. The most linearly unstable modes with the

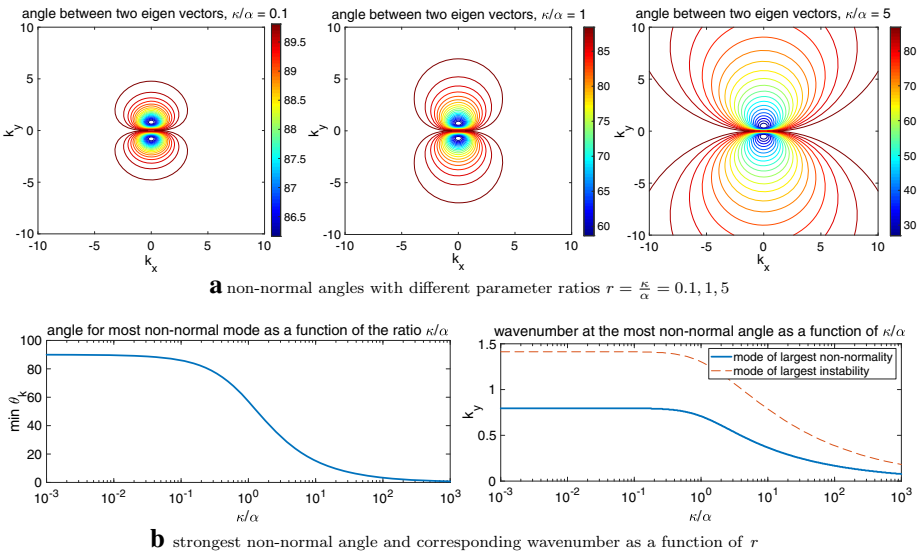

Fig. 1 The angle between the stable and unstable eigenvectors from the linear stability analysis. The first row shows the non-normal angles (in degrees) with different ratios $r = \frac{\kappa}{\alpha}$. The second row compares the strongest non-normal angle (minimum $\theta_{\mathbf{k}}$) and the corresponding wavenumber k_y as a function of r

maximum growth rate are also along the $k_x = 0$ axis for pure drift waves, aligned with the most non-normal modes (see Fig. 2 of [20] for the growth rate from linear instability). The lower row compares the most non-normal angle as a function of r. The two modes become aligned with each other as r grows to large values. Also the location of the most non-normal modes approaches the largest scale along the $k_x = 0$ axis. In conclusion, the two eigendirections become orthogonal at the limit $\kappa = 0$, and the the eigendirections get aligned in the same direction at the other limit $\alpha = 0$. Next in Sects. 3 and 4, we will focus on the limiting performances of the two extremes at the orthogonal limit $r \to 0$ and the non-normal limit $r \to \infty$.

2.2 Conserved quantities from the total energy and enstrophy equations

The linear instability is dominant in the starting transient state to excite the non-zonal fluctuation modes. As the amplitudes along the stable and unstable direction grow in time, the nonlinear effect will gradually take over to give a larger contribution. Then, the conserved quantities invariant under the nonlinear operators provide an important tool for the analysis of the evolution of the solutions incorporating both linear and nonlinear effects. Here, we first summarize the useful conservation law equations for the total energy E and total potential enstrophy W.

We can define the *total energy* E and *total potential enstrophy* W for the BHW model (1) as well as the energy and enstrophy inside the zonal state $\overline{E}$ and $\overline{W}$ in the following forms:

$$\begin{aligned} E &= \frac{1}{2}\int \left(|\nabla\varphi|^2 + n^2\right), \quad \overline{E} = \frac{1}{2}\int \overline{v}^2 = \frac{1}{2}\int |\partial_x\overline{\varphi}|^2, \\ W &= \frac{1}{2}\int q^2 = \frac{1}{2}\int \left(\nabla^2\varphi - \hat{n}\right)^2, \quad \overline{W} = \frac{1}{2}\int \overline{q}^2 = \frac{1}{2}\int \left|\partial_x^2\overline{\varphi}\right|^2. \end{aligned} \tag{12}$$

Above, $\bar{E}$, $\bar{W}$ are the energy/enstrophy from the zonal mean state with $\overline{q} = \partial_x^2 \overline{\varphi}$. Note that the enstrophy W in the BHW model is defined based on the balanced potential vorticity $q = \nabla^2 \varphi - \tilde{n}$. Through the construction of the BHW model (1), the nonlinear advection terms conserve both the energy and the balanced enstrophy. The dynamical equations for the total energy and potential enstrophy can be derived in the following equations:

$$\begin{aligned} \frac{\mathrm{d}E}{\mathrm{d}t} &= \int (\kappa + \overline{v})\, \overline{\tilde{u}\tilde{n}} - \alpha \int (\tilde{n} - \tilde{\varphi})^2 \; - D_E, \\ \frac{\mathrm{d}W}{\mathrm{d}t} &= \kappa \int \overline{\tilde{u}\tilde{n}} \; - D_W, \end{aligned} \tag{13}$$

In the above equations, the last terms D_E, D_W represent the dissipation effect μ in the total energy and enstrophy

$$\begin{aligned} D_E &= \mu \int \left(|\Delta \varphi|^2 + |\nabla n|^2 \right), \\ D_W &= \mu \int |\nabla q|^2 . \end{aligned}$$

The additional term due to the mean velocity $\overline{v} = \partial_x \overline{\varphi}$ advection in the energy equation represents the zonal flow transport of the particle flux, $\overline{\tilde{u}\tilde{n}}$. One negative-definite term due to the non-adiabatic resistivity α appears in the total energy E equation as an additional energy sink, while the drift factor α has no effect on the change of total enstrophy W. More generalized formulation with inhomogeneous dissipations can be found in Section III of [14].

Besides, we can find the dynamical equations for the zonal energy and enstrophy. The equations for the zonal mean states $\overline{q}\,(x) = \partial_x^2 \overline{\varphi}\,(x)$ and $\overline{n}\,(x)$ in the BHW model can be derived as

$$\begin{aligned} \partial_t \overline{q} + \partial_x \left(\overline{\tilde{u}\tilde{q}} \right) &= \mu \partial_x^2 \overline{q}, \\ \partial_t \overline{n} + \partial_x \left(\overline{\tilde{u}\tilde{n}} \right) &= \mu \partial_x^2 \overline{n}. \end{aligned} \tag{14}$$

The adiabaticity α is only applied on the fluctuation components with tildes, so it has no contribution on the zonal mean equations. The right hand sides of (14) are due to the homogeneous damping terms. The fluctuation feedback to the zonal mean state is through the nonlinear coupling term as an eddy diffusivity effect

$$\partial_x \left(\overline{\tilde{u}\tilde{f}} \right) = \frac{1}{L_y} \int \left(\tilde{\varphi}_x \tilde{f}_y - \tilde{\varphi}_y \tilde{f}_x \right) \mathrm{d}y,$$

with $\tilde{f} = \tilde{q}, \tilde{n}$. The relation between the vorticity eddy flux $\overline{\tilde{u}\tilde{q}}$ and the particle density flux $\overline{\tilde{u}\tilde{n}}$ can be computed using the definition of zonal and poloidal velocity $\tilde{u} = -\partial_y \varphi, \tilde{v} = \partial_x \tilde{\varphi}$

$$\overline{\tilde{u}\tilde{q}} = \int \tilde{u} \left(\frac{\partial^2 \tilde{\varphi}}{\partial x^2} - \tilde{n} \right) \mathrm{d}y = -\overline{\tilde{u}\tilde{n}} + \partial_x \left(\overline{\tilde{u}\tilde{v}} \right), \tag{15}$$

where in the secondary equality we use integration by parts

$$\overline{\tilde{u}\partial_x \tilde{v}} = -\overline{\partial_y \tilde{\varphi}\, \partial_x^2 \tilde{\varphi}} = \partial_x \left(\overline{\tilde{u}\tilde{v}} \right).$$

Especially, the second term on the right hand side will vanish when another integration along x is applied. The total fluxes in vorticity and density are related to opposite signs as

$$\int \left(\overline{\tilde{u}\tilde{q}} \right) \mathrm{d}x = - \int \left(\overline{\tilde{u}\tilde{n}} \right) \mathrm{d}x.$$

Using the above relations, the dynamical equation for the zonal mean energy and enstrophy can be found directly from the equations for the mean states

$$\begin{aligned} \frac{\mathrm{d}\overline{E}}{\mathrm{d}t} &= -\int \bar{v}\left(\overline{\tilde{u}\tilde{q}}\right) - \mu \int |\partial_x \bar{v}|^2, \\ \frac{\mathrm{d}\overline{W}}{\mathrm{d}t} &= \int \partial_x^2 \bar{v}\left(\overline{\tilde{u}\tilde{q}}\right) - \mu \int |\partial_x \tilde{q}|^2. \end{aligned} \tag{16}$$

From the above Eq. (16), we observe that the interactions between the zonal velocity $\bar{v}$ and the vorticity flux $\overline{\tilde{u}\tilde{q}}$ play the central role of energy and enstrophy transfers between the zonal state and the non-zonal fluctuations.

3 Zero background density gradient regime with $\kappa = 0$

The BHW model (1) in general incorporates various model effects including dissipation, non-adiabatic resistivity, as well as the nonlinear drift wave–zonal flow interaction [8,21,24]. These different factors lead to very complicated final model dynamics and rich phenomena. A convenient way to understand the coupled effects is to consider the limiting regimes of the model where the individual contribution from each component can be separated. In this way, we are able to concentrate on the mechanisms from different parameter regimes and gain a better understanding of the combined effects leading to the distinctive phenomena observed in plasma edge turbulence. Especially, we are interested in the change in dynamics due to the non-adiabatic resistivity parameter α and the background density gradient κ.

In this section, we first focus on interactions between the two eigendirections at the zero background density limit $\kappa = 0$. At this limit, the original BHW model (1) is simplified to the form without drift waves

$$\begin{aligned} &\frac{\partial q}{\partial t} + \nabla^{\perp}\varphi \cdot \nabla q = \mu \Delta q, \\ &\frac{\partial n}{\partial t} + \nabla^{\perp}\varphi \cdot \nabla n = \alpha\left(\tilde{\varphi} - \tilde{n}\right) + \mu \Delta n. \end{aligned} \tag{17}$$

This limit, $r = \kappa/\alpha \to 0$, refers to a regime with dominant adiabaticity α where the linear instability is eliminated. The integrable solutions in the stable and unstable subspaces can be achieved. Thus, we are able to analyze explicitly on the linear and nonlinear coupling between the two eigendirections. Still, the simplified dynamics (17) contains many interesting processes to be investigated.

3.1 Explicit integrable dynamics at the limit $\kappa = 0$

At the zero background density $\kappa = 0$, no linear instability exists to generate positive growth rate. Directly from the expressions in (8) for the eigenvalues, the unstable branch becomes a metastable one with zero dispersion relation $\omega^{+} = 0$, while the stable branch becomes purely imaginary $\omega^{-} = -i\alpha\left(1 + k^{-2}\right)$ with no dispersive drift waves. The linear coupling from the resistivity factor α cannot change in energy in the metastable branch ω^{+}, while the nonlinear coupling effect transfers the energy to the stable branch ω^{-} to get damped. This simple structure enables us to focus on the explicit energy exchanges between the two subdirections characterized by the two eigenvectors.

By carrying out the same eigenvalue decomposition of the linear matrix for each wavenumber $\mathbf{k}$, the system (17) contains one metastable direction with zero eigenvalue and one stable direction with negative eigenvalue. Thus, the following two subspaces can be discovered:

- *metastable direction* with $\omega^+ = 0$: the density $\hat{n}^+ = \hat{\varphi}^+$, and the potential vorticity becomes $\hat{q}^+ = -\left(k^2+1\right)\hat{\varphi}^+$;
- *stable direction* with $\omega^- = -i\alpha\left(1+k^{-2}\right)$: the density $\hat{n}^- = -k^2\hat{\varphi}^-$, and the potential vorticity vanishes $\hat{q}^- = -k^2\hat{\varphi}^- - \hat{n}^- = 0$.

Thus, the full potential function in the non-zonal fluctuation state $\tilde{\varphi}$ can be represented by a combination of the stable and metastable modes

$$\tilde{\varphi} = \sum \left[\hat{\varphi}_{\mathbf{k}}^+ + \hat{\varphi}_{\mathbf{k}}^- e^{-\alpha\left(1+k^{-2}\right)t}\right] e^{i\mathbf{k}\cdot\mathbf{x}-\mu k^2 t}. \tag{18}$$

The linearly stable damping and homogeneous dissipation are added explicitly as an exponential decay factor in time $e^{-\alpha\left(1+k^{-2}\right)t}$ as well as the additional damping term $e^{-\mu k^2 t}$. The corresponding potential vorticity $\tilde{q}$ and particle density $\tilde{n}$ state can be also expressed in terms of the two branches $\left(\hat{\varphi}_{\mathbf{k}}^+, \hat{\varphi}_{\mathbf{k}}^-\right)$ accordingly

$$\begin{aligned} \tilde{q} &= -\sum \left(k^2+1\right)\hat{\varphi}_{\mathbf{k}}^+ e^{i\mathbf{k}\cdot\mathbf{x}-\mu k^2 t}, \\ \tilde{n} &= \sum \left[\hat{\varphi}_{\mathbf{k}}^+ - k^2\hat{\varphi}_{\mathbf{k}}^- e^{-\alpha\left(1+k^{-2}\right)t}\right] e^{i\mathbf{k}\cdot\mathbf{x}-\mu k^2 t}. \end{aligned} \tag{19}$$

Note that the potential vorticity q only contains the metastable mode φ^+, while the electrostatic potential function φ combines both the stable and metastable components. In fact, the metastable state $\hat{q} = -\left(k^2+1\right)\hat{\varphi}^+$ represents the potential vorticity $q^{\mathrm{HM}} = \nabla^2\varphi - \tilde{\varphi}$ in the one-field Hasegawa–Mima (HM) model (3) at the adiabatic limit $\alpha \to \infty$.

Therefore, using the two eigendirections, we can directly decouple the *HM state* $\hat{q}$ at the adiabatic limit, while the additional effect $\hat{\varphi}^-$ introduces the additional non-adiabatic effect from the finite resistivity $\alpha < \infty$. For direct computation of the modes for each single wavenumber k, the stable branch can be recovered from the potential vorticity q and electrostatic potential function φ mode

$$\hat{\varphi}_{\mathbf{k}}^- e^{-\alpha\left(1+k^{-2}\right)t} = \hat{\varphi}_{\mathbf{k}} - \hat{\varphi}_{\mathbf{k}}^+ = \hat{\varphi}_{\mathbf{k}} + \frac{\hat{q}_{\mathbf{k}}}{k^2+1}.$$

At the limit $\kappa = 0$, we are able to focus on the equation for potential vorticity (1a) with the feedback from n only coming from the nonlinear coupling. This shows that the limiting regime $\kappa = 0$ is a desirable case for the analysis of the additional contributions from the finite resistivity factor α.

3.1.1 Spectral equations for the metastable and stable modes

With the mode decomposition into the two branches (18) and (19), the two modes $\left(\hat{\varphi}_{\mathbf{k}}^+, \hat{\varphi}_{\mathbf{k}}^-\right)$ are further coupled from the nonlinear operator. More precisely, we can find the explicit dynamical equations for the two modes by substituting the decomposition into

the original dynamics (17)

$$\begin{aligned}
\frac{\mathrm{d}\hat{\varphi}^+_{\mathbf{k}}}{\mathrm{d}t} &= \sum_{\mathbf{m}+\mathbf{n}=\mathbf{k}} A^+_{\mathbf{mnk}}\left[\hat{\varphi}^+_{\mathbf{m}}\hat{\varphi}^+_{\mathbf{n}} + \hat{\varphi}^-_{\mathbf{m}}\hat{\varphi}^+_{\mathbf{n}} e^{-\alpha(1+n^{-2})t}\right],\\
\frac{\mathrm{d}\hat{\varphi}^-_{\mathbf{k}}}{\mathrm{d}t} &= \sum_{\mathbf{m}+\mathbf{n}=\mathbf{k}} \Big[A^{-,++}_{\mathbf{mnk}}\hat{\varphi}^+_{\mathbf{m}}\hat{\varphi}^+_{\mathbf{n}} e^{\alpha(1+k^{-2})t} + A^{-,-+}_{\mathbf{mnk}}\hat{\varphi}^-_{\mathbf{m}}\hat{\varphi}^+_{\mathbf{n}} e^{\alpha(k^{-2}-n^{-2})t}\\
&\quad + A^{-,--}_{\mathbf{mnk}}\hat{\varphi}^-_{\mathbf{m}}\hat{\varphi}^-_{\mathbf{n}} e^{\alpha(k^{-2}-n^{-2}-m^{-2})t}\Big].
\end{aligned} \tag{20}$$

Above $\{A_{\mathbf{mnk}}\}$ are the coupling coefficients between the different modes satisfying the triad relation $\mathbf{m}+\mathbf{n}=\mathbf{k}$. The homogeneous dissipation on the right hand side of the original equation can be eliminated by the explicit damping rate in (19). The coupling coefficient for the metastable mode can be found as $A^+_{\mathbf{mnk}} = -\frac{n^2+1}{k^2+1}\mathbf{m}^\perp\cdot\mathbf{n}$ and similarly for the coefficients $A^-_{\mathbf{mnk}}$ for the stable mode. In general, direct computation of the nonlinear term requires estimation among all the coupling modes throughout the spectra.

Directly from the above Eq. (20), we see the nonlinear coupling between different scales and the stable and unstable modes together. The first equation equation of (20) describes explicitly the evolution of the metastable state $\hat{\varphi}^+$ (that is, the HM state $\hat{q}$). At the adiabatic limit $\alpha\to\infty$, the second coupling term on the right hand side, $\hat{\varphi}^-_{\mathbf{m}}\hat{\varphi}^+_{\mathbf{n}} e^{-\alpha(1+n^{-2})t}$, between the two subdirections vanishes due to the strong damping in time. The equation reduces exactly to the one-layer HM model (3)

$$\frac{\mathrm{d}\hat{q}_{\mathbf{k}}}{\mathrm{d}t} = \sum_{\mathbf{m}+\mathbf{n}=\mathbf{k}} A^+_{\mathbf{mnk}}\hat{\varphi}^+_{\mathbf{m}}\hat{q}^+_{\mathbf{n}} = -\left(\nabla^\perp\varphi^+\cdot\nabla q\right)_{\mathbf{k}},$$

which models the adiabatic dynamics with no resistivity $\alpha=\infty$. On the other hand, with finite non-adiabatic resistivity $\alpha<\infty$, the stable mode $\hat{\varphi}^-$ extracts additional energy in the HM mode $\hat{\varphi}^+$ through the second coupling term to relocate the energy spectrum. The single role of the one-field HM state q with the finite resistivity effect α introduced from an unstable forcing is discussed in [20]. There the solution becomes gradually unstable as the value of α decreases (see Fig. 6 in [20]) due to the lack of energy transfer and dissipation mechanism from the stable φ^- branch.

3.1.2 The enstrophy and energy equations

The total energy and enstrophy equations in (12) provide a convenient way to quantify the total amount of variability among the spectral modes. Especially, the complicated nonlinear coupling effects will not change the total energy and enstrophy structure of the system as shown in the dynamics (13). In the limiting regime with $\kappa=0$, the expressions for total energy and enstrophy can be further simplified through the decomposition between the two states (19). Using the explicit formulas for the decoupled states $\left(\hat{\varphi}^+,\hat{\varphi}^-\right)$, we can rewrite the conserved total enstrophy and energy as

$$\begin{aligned}
W &= \frac{1}{2}\int q^2 = \frac{1}{2}\sum\left(k^2+1\right)^2\left|\hat{\varphi}^+_{\mathbf{k}}\right|^2,\\
E &= \frac{1}{2}\int |\nabla\varphi|^2 + n^2 = \frac{1}{2}\sum\left(k^2+1\right)\left|\hat{\varphi}^+_{\mathbf{k}}\right|^2 + k^2\left(k^2+1\right)\left|\hat{\varphi}^-_{\mathbf{k}}\right|^2 e^{-2\alpha(1+k^{-2})t}.
\end{aligned} \tag{21}$$

Again the enstrophy W related to the potential vorticity q is only determined by the metastable HM state with $\omega^+ = 0$, while the total energy E also includes the contribution from the other branch of stable mode with a damping factor $\sigma^- = -\alpha\left(1 + k^{-2}\right)$. The total kinetic energy and energy in the density need to be decomposed into the two branches

$$k^2 |\hat{\varphi}|^2 = k^2 \left|\hat{\varphi}^+\right|^2 + 2k^2 \mathfrak{Re}\left(\hat{\varphi}^+ \hat{\varphi}^{-*}\right) e^{-\alpha\left(1+k^{-2}\right)t} + k^2 \left|\hat{\varphi}^-\right|^2 e^{-2\alpha\left(1+k^{-2}\right)t},$$
$$|\hat{n}|^2 = \left|\hat{\varphi}^+\right|^2 - 2k^2 \mathfrak{Re}\left(\hat{\varphi}^+ \hat{\varphi}^{-*}\right) e^{-\alpha\left(1+k^{-2}\right)t} + k^4 \left|\hat{\varphi}^-\right|^2 e^{-2\alpha\left(1+k^{-2}\right)t}.$$

Therefore, the cross-term gets cancelled in the total energy as a combination of the stable and metastable states

$$k^2 |\hat{\varphi}|^2 + |\hat{n}|^2 = \left(k^2+1\right)\left|\hat{\varphi}^+\right|^2 + k^2\left(k^2+1\right)\left|\hat{\varphi}^-\right|^2 e^{-2\alpha\left(1+k^{-2}\right)t}.$$

Together with the enstrophy in each mode, $W_k = |\hat{q}_{\mathbf{k}}|^2 = \left(k^2+1\right)^2 \left|\hat{\varphi}^+_{\mathbf{k}}\right|^2$, the energy in the stable subspace can be recovered by

$$E_k^- = k^2 \left|\hat{\varphi}^-_{\mathbf{k}}\right|^2 = \frac{e^{2\alpha\left(1+k^{-2}\right)t}}{k^2+1}\left(E_k - \frac{W_k}{k^2+1}\right), \tag{22}$$

with $E_k = k^2 |\hat{\varphi}_k|^2 + |\hat{n}_k|^2$ and $W_k = |\hat{q}_k|^2$ the energy and enstrophy at each scale k. Using the above relation, we can explicitly compute the energy inside the stable and metastable subspaces and check their interactions for the energy exchange along scales.

From the enstrophy Eq. (13) at the limit $\kappa = 0$, it is notable that the total enstrophy W becomes a conserved quantity only subject to the dissipation effect

$$\frac{\mathrm{d}W}{\mathrm{d}t} = -D_W = -\mu \sum k^2 \left(k^2+1\right)^2 \left|\hat{\varphi}^+_{\mathbf{k}}\right|^2. \tag{23}$$

Without the dissipation $\mu = 0$, the total enstrophy $W = \frac{1}{2}\sum |\hat{q}_{\mathbf{k}}|^2$ is conserved in time. The detailed equation for the enstrophy at each wavenumber W_k can be also computed based on the spectral Eq. (20)

$$\frac{\mathrm{d}}{\mathrm{d}t}|\hat{q}_{\mathbf{k}}|^2 = -\left(k^2+1\right)^2 \sum_{\mathbf{m}+\mathbf{n}=\mathbf{k}} A^+_{\mathbf{mnk}}\left[\hat{\varphi}^+_{\mathbf{m}}\hat{\varphi}^+_{\mathbf{n}}\hat{\varphi}^{+*}_{\mathbf{k}} + \hat{\varphi}^-_{\mathbf{m}}\hat{\varphi}^+_{\mathbf{n}}\hat{\varphi}^{+*}_{\mathbf{k}} e^{-\alpha\left(1+m^{-2}\right)t}\right].$$

The right hand side of the above equation redistributes the energy in each mode along the scales through the triad coupling between modes $\mathbf{m}+\mathbf{n}=\mathbf{k}$. The total energy E combining both the metastable and stable modes is not conserved in time due to the parameter α introducing one additional damping

$$\begin{aligned}\frac{\mathrm{d}E}{\mathrm{d}t} &= -\alpha \int (\tilde{n} - \tilde{\varphi})^2 \; - D_E \\ &= -\alpha \sum \left(k^2+1\right)^2 \left|\hat{\varphi}^-\right|^2 e^{-2\alpha\left(1+k^{-2}\right)t} - D_E.\end{aligned} \tag{24}$$

Importantly, the negative definite resistivity effect only comes from the nonzero stable mode φ^- representing the system deviation from the adiabatic HM state. This is consistent with the intuition due to the finite particle resistivity $\alpha < \infty$ from the two-state HW model. The last term D_E on the right hand side gives the combined dissipation effect

$$D_E = \mu \sum k^2\left(k^2+1\right)\left[\left|\hat{\varphi}^+\right|^2 + k^2\left|\hat{\varphi}^-\right|^2 e^{-2\alpha\left(1+k^{-2}\right)t}\right].$$

The resistive term due to α in the energy equation vanishes as $\alpha \to \infty$. Therefore, the total energy returns to its conserved form at the adiabatic limit (see Section 2 of [21] for the conserved energy in the one-field HM system).

On top of the fluctuation states, we also need to consider the contributions from zonal states $\bar{q} = \partial_x^2 \bar{\varphi} = \partial_x \bar{v}$ for the zonal modes $k_y = 0$ as in (16). The energy and enstrophy distribution will be altered in time further through the interactions between the zonal and non-zonal states as well as the nonlinear coupling between the two subdirections. It is shown based on the one-field HM model that selective decay [21] and secondary instability [22] play an important role in transferring the fluctuation energy to zonal states and forming a dominant large-scale zonal jets. Next, we consider these different effects individually on the two-field BHW model with finite resistivity from α. First the total dissipation as a selective decay effect is analyzed; then, we consider the interactions among the fluctuation modes along the two characteristic directions; and at last to further introduce the coupling between the zonal and non-zonal state for the generation of dominant zonal jets.

3.2 Direction of energy cascade from particle resistivity and dissipation

From the previous discussion of the explicit Eq. (20) for the metastable and stable modes, we see that different scales are coupled together through the nonlinear interactions. One direct question to ask is how the resistivity and diffusion effects modify the energy spectrum with induced the forward and backward energy cascade along the scales. Here, we use the strategy of selective decay [15,21] to find *a priori* estimates for the energy transfer due to the different effects from the model.

To characterize energy transfer among different scales, the *Dirichlet quotient* is defined as the ratio between the enstrophy and energy

$$\Lambda(t) = \frac{W(t)}{E(t)} = \frac{\int \left(\nabla^2 \varphi - \tilde{n}\right)^2}{\int |\nabla \varphi|^2 + n^2}. \tag{25}$$

This ratio $\Lambda(t)$ quantifies the rates of change in energy among the wavenumbers. We can track the nonlinear exchange of energy through scales by observing the evolution of the Dirichlet quotient $\Lambda(t)$ in time. The decrease in value of $\Lambda(t)$ implies the accumulation of energy among the large scale in small wavenumber k (noting that the enstrophy W adds stronger weight on smaller scales), while the increase of $\Lambda(t)$ means the forward cascade of energy to smaller scales with a large wavenumber k. By tracking the change in the value of Λ, we can determine the energy transfer direction from the competition between the resistivity effect due to α and the above selective decay effect due to μ.

Here, we first summarize the major conclusion according to the effect on the Dirichlet quotient Λ in the following proposition:

Proposition *The energy exchanges between scales in the two-field BHW model* (17) *with zero background density gradient* $\kappa = 0$ *are subject to the three factors of dissipation, particle resistivity in fluctuations, and the mean flow interaction with a zonal state. More precisely, we can show that:*

- *The homogeneous dissipations* $\mu \Delta q$ *and* $\mu \Delta n$ *on the vorticity and density field enhance the selective decay process to drive backward energy cascade from small fluctuation modes to the leading large-scale state;*
- *The non-adiabatic resistively in fluctuation modes,* $\alpha(\tilde{\varphi} - \tilde{n})$*, acts inversely as the reversed select decay process to induce forward energy cascade from large-scale states*

to the smallest resolved mode. This process excites the small-scale fluctuations and strong particle transport;

– *The formation of a zonal velocity state $\bar{v}$ can effectively block the above forward energy cascade to small scales through the nonlinear interaction with fluctuation modes. A strong zonal mean flow will reduce the rate of energy transfer to the smallest scale and stabilize the flow solution.*

In the two-field BHW model case, multiple factors with opposite effects will act together to create the complicated turbulent solutions. We can no longer find the clean convergence result as in the one-field HM case [21]. We will first discuss the above conclusions based on the dynamical equation for Λ and heuristic implications from the BHW model. The energy exchange mechanisms from the three factors are further confirmed through direct numerical simulations.

3.2.1 Selective decay due to the dissipative effect

Selective decay principle [15] is developed based on a faster decay rate of the enstrophy from the dissipation with a relatively conserved energy during a suitable time scale. It shows the emergence of a single-mode large-scale zonal state in time through a stronger dissipation among the all the other smaller-scale modes. This infers the inverse cascade of energy from small scales to a dominant large-scale mode. The selective decay in the one-field HM models (3) purely due to the dissipation effect is discussed in [21] (see Theorem 2 there with rigorous proof of the convergence). Still the HM model only includes the adiabatic mode φ^+ at the limit $\alpha \to \infty$. Here, as a further step, we carry out a more detailed investigation for the additional effect from finite resistivity $\alpha < \infty$ of the two-field model including the coupling between the two states q and n.

Following the selective decay analysis in [21], we first consider the role of dissipation effect on the two-field BHW model (17) at the $\kappa = 0$ limit. The selective decay state due to dissipation refers to the critical point solution of minimized enstrophy W on the lowest energy shell E. This can be achieved from the variational principle with the Lagrangian multiplier. It predicts that the critical solution as the selective state contains one single wavenumber for the large-scale zonal state. The similar candidate critical state for the BHW model is computed in "Appendix A."

To be more precise, we need to show that the long time solution approaches toward this single-mode large-scale state due to the dissipation effect. This requires tracking the dynamics of the Dirichlet quotient $\Lambda(t)$. Clearly, we first have a positive lower bound for $\Lambda(t) > 0$. So we just need to show that $\Lambda(t)$ becomes monotonically decreasing from the dissipation effect to converge to a single-mode critical state solution (rigorous proof for the convergence to a single-mode zonal solution is shown in Section 5 of [21]). The dynamical equation for the Dirichlet quotient can be computed directly from the equations for W and E

$$\frac{\mathrm{d}\Lambda}{\mathrm{d}t} = \frac{1}{E^2}\left(E\dot{W} - W\dot{E}\right) = \frac{1}{E}\left(\dot{W} - \Lambda\dot{E}\right). \tag{26}$$

Here, we purely consider the contributions from the dissipation factor μ. Using the equations for the enstrophy (23) and energy (24), the right hand side of (26) can be found

as

$$\begin{aligned}\dot{W} - \Lambda\dot{E} &= -D_W + \Lambda D_E \\ &= \mu \sum \Lambda k^2 \left(k^2+1\right)\left[\left|\hat{\varphi}_k^+\right|^2 + k^2 E_k^-\right] \\ &\quad - \mu \sum k^2 \left(k^2+1\right)^2 \left|\hat{\varphi}_k^+\right|^2,\end{aligned}$$

using the explicit expressions in (19) and denoting the energy in the stable subdirection $E_k^- = k^2 \left|\hat{\varphi}_k^-\right|^2 e^{-2\alpha\left(1+k^{-2}\right)t}$ for simplicity. Further, the Dirichlet quotient can be written explicitly as

$$\Lambda(t) = \frac{\sum \left(k^2+1\right)^2 \left|\hat{\varphi}_k^+\right|^2}{\sum \left(k^2+1\right)\left(\left|\hat{\varphi}_k^+\right|^2 + E_k^-\right)}.$$

Combining the above relations together and reorganizing between the summations, we find

$$\begin{aligned}\mu^{-1}\left(\dot{W} - \Lambda\dot{E}\right) &= \frac{\sum k^2\left(k^2+1\right)\left(\left|\hat{\varphi}_k^+\right|^2 + k^2 E_k^-\right)\sum \left(k^2+1\right)^2\left|\hat{\varphi}_k^+\right|^2}{\sum \left(k^2+1\right)\left(\left|\hat{\varphi}_k^+\right|^2 + E_k^-\right)} \\ &\quad - \sum_k k^2\left(k^2+1\right)^2\left|\hat{\varphi}_{\mathbf{k}}^+\right|^2 \\ &= \sum_k \left(k^2+1\right)^2\left|\hat{\varphi}_k^+\right|^2\left[\frac{\sum_m m^2\left(m^2+1\right)\left(\left|\hat{\varphi}_m^+\right|^2 + E_m^-\right)}{\sum_m \left(m^2+1\right)\left(\left|\hat{\varphi}_m^+\right|^2 + E_m^-\right)} - k^2\right] \\ &= \sum_k \left(k^2+1\right)^2\left|\hat{\varphi}_k^+\right|^2\left[\frac{\sum_m \left(m^2-k^2\right)\left(m^2+1\right)\left(\left|\hat{\varphi}_m^+\right|^2 + E_m^-\right)}{\sum_m \left(m^2+1\right)\left(\left|\hat{\varphi}_m^+\right|^2 + E_m^-\right)}\right] \\ &= C^{-1}\sum_{k,m}\left(m^2-k^2\right)\left(k^2+1\right)^2\left(m^2+1\right)\left|\hat{\varphi}_k^+\right|^2 \\ &\quad \times\left(\left|\hat{\varphi}_m^+\right|^2 + m^2\left|\hat{\varphi}_m^-\right|^2 e^{-2\alpha\left(1+m^{-2}\right)t}\right) \\ &\le -C^{-1}\sum_{k>m}\left(m^2-k^2\right)^2\left(k^2+1\right)\left(m^2+1\right)\left|\hat{\varphi}_k^+\right|^2\left|\hat{\varphi}_m^+\right|^2 + C_1 e^{-2\alpha t}.\end{aligned}$$

Above we bring outside the constant $C = \sum_m \left(m^2+1\right)\left(\left|\hat{\varphi}_m^+\right|^2 + E_m^-\right) > 0$. The double summation is rearranged, and we exchange the order of summations for m and k. The first component on the right hand side only involves interactions between the metastable HM mode φ^+, which leads to a negative definite damping effect using the symmetry in coefficients. The second component involving cross-interactions between φ^+ and φ^- can be limited as small as possible for large enough time $t > T$ due to the strong exponential decay $e^{-2\alpha t}$ from the stable mode. The above result is consistent with the selective decay in the one-field model at the adiabatic limit $\alpha \to \infty$ [21] where the second term from finite resistivity vanishes.

Therefore, after long enough time $t > T$, the positive part due to φ^- on the right hand side above will be reduced to small enough value, so that we have from the dissipation effect $\mu > 0$

$$\frac{\mathrm{d}\Lambda}{\mathrm{d}t} < 0. \tag{27}$$

Then, the Dirichlet quotient becomes strictly monotonically decreasing afterward. This characterizes the energy transfer from the small-scale modes to the large scale purely from the dissipation μ. Further, it can be shown that the solution will always converge to a selective decay state with a purely zonal state with a single wavenumber. In fact, a single wavenumber zonal state solution $\bar{v} = \bar{v}_k e^{ik_x x}$ gives the Dirichlet quotient

$$\overline{\Lambda}^* = \frac{\int |\partial_x \bar{v}|^2}{\int \bar{v}^2 + \bar{n}^2} \le \frac{k_x^2 |\bar{v}_k|^2}{|\bar{v}_k|^2} = \left(\frac{2\pi}{L_x}\right)^2 n_x^2 < 1, \tag{28}$$

where n_x is an integer for the wavenumber $k_x = \frac{2\pi}{L_x} n_x$, and the zonal flow is always in a large-scale mode. Adding a small-scale fluctuation $\hat{\varphi}_k^*$ on top of the above single-mode solution will always increase the quotient, that is,

$$\frac{k_x^2 |\bar{v}_k|^2 + \left(k^2+1\right)^2 |\hat{\varphi}_k|^2}{|\bar{v}_k|^2 + \left(k^2+1\right)|\hat{\varphi}_k|^2} - \overline{\Lambda}^* = \frac{\left(k^2+1-k_x^2\right)\left(k^2+1\right)|\hat{\varphi}_k|^2 |\bar{v}_k|^2}{\left[|\bar{v}_k|^2 + \left(k^2+1\right)|\hat{\varphi}_k|^2\right]|\bar{v}_k|^2} > 0.$$

This infers that the Dirichlet quotient Λ will keep decay to a smaller value level due to (27) with purely zonal state if there exist nonzero fluctuation modes $\hat{\varphi}_k$. This conclusion is in general true if the quotient Λ becomes monotonically decreasing in time.

With the dissipation effect to be dominant, the selective decay guarantees the convergence to a single-mode zonal state (as illustrated in Fig. 3 of [21]). In addition, from the above derivation we also see the different roles of the two eigenmodes, φ^+, φ^- during the decaying process. The metastable HM mode interaction $\hat{\varphi}_{\mathbf{m}}^+ \hat{\varphi}_{\mathbf{n}}^+$ in (20) gives the negative damping to decrease the Dirichlet quotient Λ, while the coupling effect due to $\hat{\varphi}_{\mathbf{m}}^+ \hat{\varphi}_{\mathbf{n}}^-$ may act to increase the quotient Λ to reduce the rate of inverse cascade in the transient state. This further confirms the role of the stable mode φ^- in the two-field model to generate stronger nonlinear particle transport that is not modeled in the one-field HM system [20].

3.2.2 Reversed selective decay due to finite resistivity

Next we consider the resistive particle interactions due to the parameter α separately among the fluctuation modes and assume no zonal state in the model first, $\bar{v} = \bar{n} = 0$. From the energy Eqs. (23) and (24) without dissipation, the total energy E is decaying in time while the total enstrophy W stays conserved. This acts reversely in contract to the previous selective decay effect from the dissipation, implying that the energy cascades to smaller scales to create more vortical fluctuations. This critical solution with minimized energy E at a constant enstrophy W can be directly computed from the variational principle shown in "Appendix A."

In this case, we focus on the contribution from the finite value of $0 < \alpha < \infty$. The dynamical equation for the ratio Λ can be derived in a similar fashion using the two Eqs. (23) and (24)

$$\begin{aligned} \frac{\mathrm{d}\Lambda}{\mathrm{d}t} &= -\frac{\Lambda}{E}\dot{E} = \frac{\alpha\Lambda}{E}\int (\tilde{n}-\tilde{\varphi})^2 \\ &= \frac{\alpha\Lambda}{E}\sum \left(k^2+1\right)\left|\hat{\varphi}_k^-\right|^2 e^{-2\alpha\left(1+k^{-2}\right)t} > 0. \end{aligned} \tag{29}$$

In the above equation, only the contribution from the resistive parameter α is considered without any damping terms to exclude the effect of the dissipative selective decay. In contrast to the selective decay case from the dissipation μ, the parameter α acts to increase

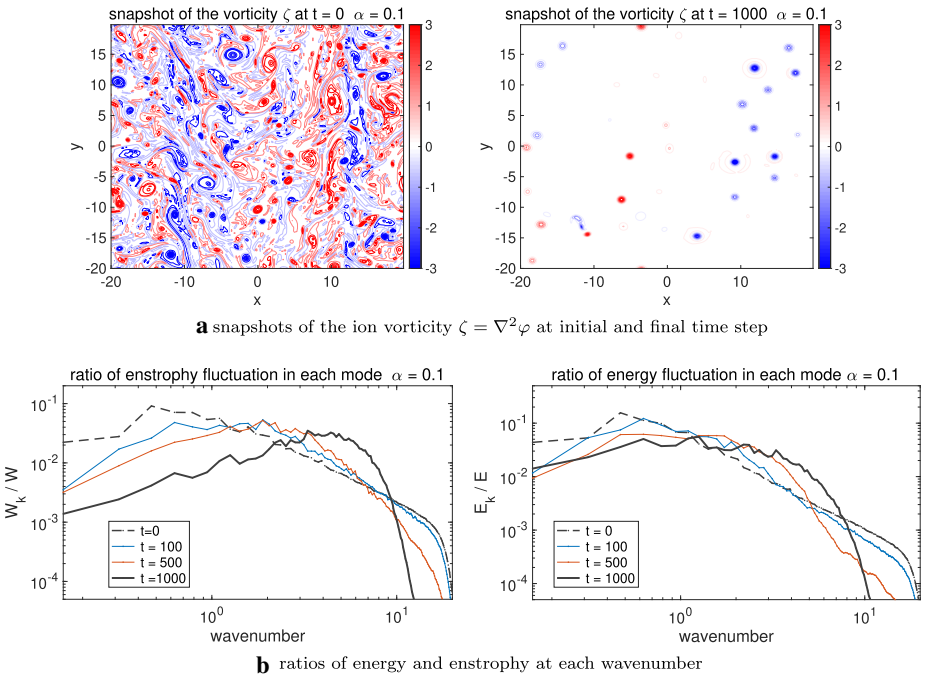

Fig. 2 Flow simulation result with small $\alpha = 0.1$ in the limiting regime $\kappa = 0$. The flow starts from the steady-state solution using $\kappa = 1, \alpha = 0.1$ (upper left), and the final solution at $t = 1000$ is dominated by small-scale vortical modes (upper right). The lower panel compares the normalized enstrophy spectrum, W_k/W, and energy spectrum, E_k/E, measured at different time instants during the system evolution to show the direction of energy transport. The initial spectra are plotted in dashed line in comparison with the final time spectra in solid black line

the value of the Dirichlet quotient. This increase in value of Λ refers to the 'reversed selected decay,' where the energy is transferring from the large-scale modes to the small fluctuation scales. The increasing value of the Dirichlet quotient $\Lambda(t)$ is also linked to the induction of strong particle transport as α goes to small values.

For the final converged state, it can be found that the increasing Dirichlet quotient Λ has an upper bound in the Galerkin truncated model

$$\begin{aligned}\Lambda(t) &= \frac{\sum (k^2+1)^2 \left|\hat{\varphi}_k^+\right|^2}{\sum (k^2+1) \left|\hat{\varphi}_k^+\right|^2 + k^2 (k^2+1) \left|\hat{\varphi}_k^-\right|^2 e^{-2\alpha(1+k^{-2})t}} \le \frac{\sum (k^2+1)^2 \left|\hat{\varphi}_k^+\right|^2}{\sum (k^2+1) \left|\hat{\varphi}_k^+\right|^2} \\ &= \frac{W^+}{E^+} \le K^2 + 1,\end{aligned}$$

with K the maximum truncated wavenumber in the spectral model. In fact, for large wavenumbers k, the dissipation effect μk^2 will finally take over to overwhelm the effect from α in the smallest scales. Combined with (29), this shows that the Directly quotient $\Lambda(t)$ is the monotonically increasing with an upper bound. This guarantees the reserve selective decay effect for the energy to keep going downscale to the smaller scale with the largest wavenumber $k = K$ driven by the nonzero stable mode φ^-. This reversed selective decay process is confirmed from direct numerical simulation shown in Fig. 2 in next section.

In addition, the rate of growth of Λ is determined purely by the stable state φ^-, while the value of the HM state φ^+ is independent in this process. Therefore, we can illustrate

the roles of the two coupling states φ^+ and φ^- during the time evolution by the combined contributions from resistivity and dissipation. First, the stable state φ^- induces forward energy cascade and strong particle flux from large to small scales due to the reversed selective decay with α; at the same time the metastable state φ^+ transfers the energy in small scales to form a large-scale zonal state due to the selective decay from dissipation μ. In the extreme case when the energy inside the metastable subspace becomes zero, $\varphi^- \equiv 0$, the energy E only contains the metastable branch and is also conserved. The system goes to the exact HM state as shown in [21].

3.2.3 The effect of a nonzero zonal state $\bar{v} \neq 0$

Previously, we only consider the interactions between the non-zonal fluctuation modes $k_y \neq 0$. It shows the competition between the selective decay and the reversed feedback from the stable subspace. Still, one additional important factor that has not been considered in the BHW model is the interaction due to the zonal velocity $\bar{v}$ and zonal particle flux $\overline{\tilde{u}\tilde{n}}$. The zonal state $\bar{v}$ will not change the total enstrophy W, while it introduces an important additional flux term in the energy Eq. (13)

$$\frac{\mathrm{d}E}{\mathrm{d}t} = -\alpha \int (\tilde{n} - \tilde{\varphi})^2 + \int \bar{v}\left(\overline{\tilde{u}\tilde{n}}\right). \tag{30}$$

Notice that the second term on the right hand side $\int \bar{v}\left(\overline{\tilde{u}\tilde{n}}\right)$ does not appear in the MHW model without the balanced flux modification [2,24]. This leads to one important difference between the MHW and BHW models. Unlike the resistive effect due to α purely due to the stable mode φ^- as shown in the previous section, the zonal coupling term $\overline{\tilde{u}\tilde{n}}$ introduces the interaction between the metastable and stable modes φ^+, φ^-. Using the decompositions in (18) and (19), the zonal particle flux can be computed explicitly as

$$\begin{aligned}\overline{\tilde{u}\tilde{n}} &= -i \sum_{k_x = m_x + n_x} m_y \left(1 - n^2\right) \hat{\varphi}^+_{\mathbf{m}} \hat{\varphi}^-_{\mathbf{n}} e^{-\alpha\left(1+n^{-2}\right)t} e^{ik_x x} \\ &= \int \left(\partial_y \varphi^+\right)(1 + \Delta)\,\varphi^- \mathrm{d}y,\end{aligned}$$

with $\varphi^+ = \sum \hat{\varphi}^+_{\mathbf{k}} e^{i\mathbf{k}\cdot\mathbf{x}}$ and $\varphi^- = \sum \hat{\varphi}^-_{\mathbf{k}} e^{i\mathbf{k}\cdot\mathbf{x} - \alpha\left(1+k^{-2}\right)t}$ and without the self-coupling inside the modes of φ^+ and φ^-. This represents the feedback from the interactions between the two states φ^+, φ^-.

With the inclusion of the zonal state, the energy can be decomposed into the energy in the mean and the fluctuations as in (12), that is,

$$E = \bar{E} + \tilde{E}, \quad \tilde{E} = \frac{1}{2} \int |\nabla \tilde{\varphi}|^2 + \tilde{n}^2.$$

The flux interaction term can be estimated by an upper bound by directly using Cauchy's inequality, that is,

$$\int \bar{v}\left(\overline{\tilde{u}\tilde{n}}\right) \leq \int |\bar{v}| \left|\overline{\tilde{u}\tilde{v}}\right| \leq \frac{\bar{v}_m}{2} \int |\tilde{u}|^2 + |\bar{v}|^2 \leq \bar{v}_m \tilde{E}, \tag{31}$$

with $\bar{v}_m = \max_x |\bar{v}|$ as the maximum amplitude for the zonal velocity state. With the above estimation (31), an additional correction term due to the zonal state interaction should be added to the previous dynamics (29) for the Dirichlet quotient in non-dissipative case

$$\frac{\mathrm{d}\Lambda}{\mathrm{d}t} = -\frac{\Lambda}{E}\dot{E} \geq -\Lambda \bar{v}_m \frac{\tilde{E}}{E} + \frac{\alpha \Lambda}{E} \int (\tilde{n} - \tilde{\varphi})^2. \tag{32}$$

The second term on the right hand side of (32) plays the role of reserved selective decay from (29). The first term only involving the ratio of energy in fluctuation $\tilde{E}/E$ is the new feature in the BHW model, which shows that the generation of a zonal state $\bar{v}$ can prevent the persistent energy cascade all the way to the smallest scale. This further illustrates the role of a self-generated zonal jet to block the strong fluctuation particle transport [8,14, 23]. The zonal flow interaction plays the role to suppress the excitation of many small-scale structures. The formation of a strong zonal state $\bar{v}$ together with strong metastable fluctuations φ^+ may drive the Dirichlet quotient Λ decreasing in time. Combined with the selective decay from the dissipation μ, a purely zonal state as in (28) will emerge in the final converged solution (see the case with large α in Fig. 3).

On the other hand, the reversed selective decay to small scales in (26) is still valid if the right hand side of (32) stays positive. This requires a small enough zonal state $\bar{v}_m$ to allow for the forward energy cascade. We can find one sufficient condition for the forward energy cascade to be maintained as

$$\sum \left(\frac{\alpha}{\bar{v}_m} - k^2 \right) (k^2+1) \left| \hat{\varphi}_k^- \right|^2 \geq \sum (k^2+1) \left| \hat{\varphi}_k^+ \right|^2. \tag{33}$$

This is possible when there is at least one strong stable fluctuation mode $\hat{\varphi}_k^-$ with wavenumber $k < \sqrt{\frac{\alpha}{\bar{v}_m}}$. This requires a weak enough zonal state for $\max_x |\bar{v}| = \bar{v}_m < \frac{\alpha}{K^2}$.

3.3 Numerical confirmation of the energy transfers between different scales

In the last part, we confirm the conclusions for enstrophy and energy transfer from the above analysis using direct numerical simulations. We consider the model Eq. (17) with zero background density gradient $\kappa = 0$ and track the flow evolutions with various values of the adiabaticity $\alpha \in [0.1, 5]$. The effect of the dissipation is set in a much smaller value $\mu = 1 \times 10^{-4}$. In this way, we are able to focus on the competing effects from the particle resistivity (29) due to fluctuation state to induce reversed selective decay, and the interactions with the mean flow (32) to balance the forward energy cascade process.

For the numerical setup, the computational domain size is set equal in the x and y directions $L_x = L_y = 40$. In this zero density gradient regime $\kappa = 0$, no linear instability is modeled to excite the drift waves; thus, the flow solutions decay from the prescribed initial states. The test initial state is generated using the steady-state turbulent solution with $\kappa = 1$ and the same value of α. Besides, hyperviscosities $-\nu\Delta^s q$ and $-\nu\Delta^s n$ are added to the smallest scales of the potential vorticity and density fields with tiny coefficient $\nu = 7 \times 10^{-21}$ and high order $s = 8$ to dissipate the additional energy in the underresolved smallest scales. The direct numerical simulation is based on a standard pseudo-spectral scheme with $N = 256$ discretization points along each direction. A fourth-order explicit–implicit Runge–Kutta scheme is used for time integration with implicit part only for the stiff hyperviscosity term. This is the same numerical setup used previously for the BHW model simulations in [23,24].

3.3.1 Two typical regimes with different values of α

In the numerical tests, we first compare the energy exchange along different scales under different values of α. In order to track the energy cascade direction between scales, we compare the normalized enstrophy and energy spectra at different time instants during

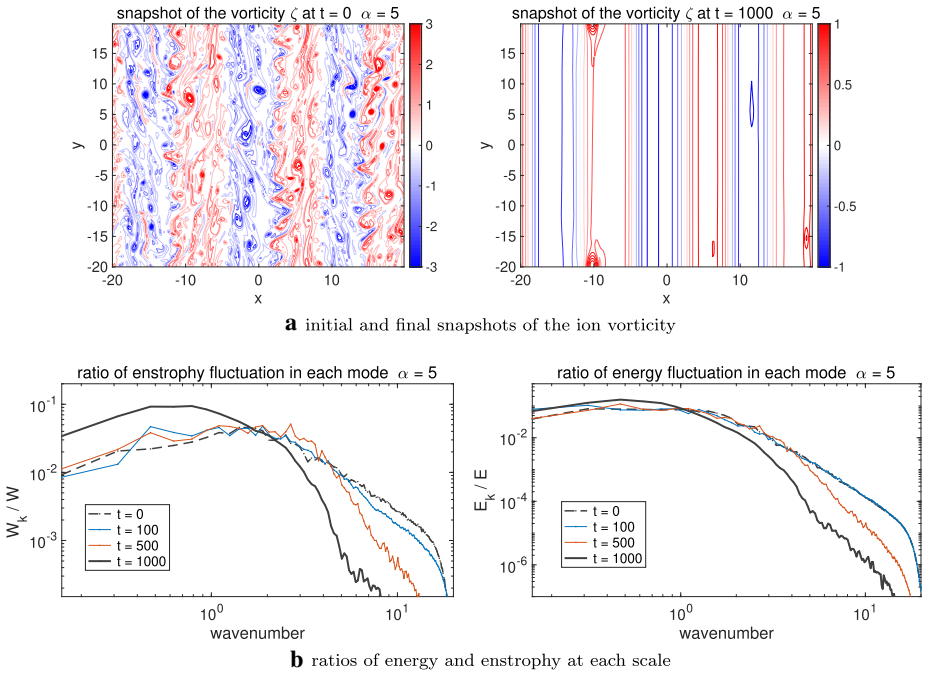

Fig. 3 Flow simulation result with large $\alpha = 5$ in the limiting regime $\kappa = 0$. The flow starts from the steady-state solution using $\kappa = 1, \alpha = 5$ (upper left), and the final solution at $t = 1000$ is dominated by a large-scale zonal flow (upper right). The lower panel compares the normalized enstrophy spectrum, W_k/W, and energy spectrum, E_k/E, measured at different time instants to show the direction of energy transport. The initial spectra are plotted in dashed line in comparison with the final time spectra in solid black line

the evolution of the solution by computing the ratios

$$\frac{W_k}{W} = \frac{|\hat{q}_k|^2}{\sum_k |\hat{q}_k|^2}, \quad \frac{E_k}{E} = \frac{k^2 |\hat{\varphi}_k|^2 + |\hat{n}_k|^2}{\sum_k k^2 |\hat{\varphi}_k|^2 + |\hat{n}_k|^2}.$$

The enstrophy W according to (23) is only damped by the weak dissipation term $\mu = 1 \times 10^{-4}$, while the resistivity parameter α has no effect on changing the value of total enstrophy. On the other hand, the total energy is not conserved even without the dissipation effect. The total energy E is subject to the additional effect due to the resistivity parameter α in (29). Strong damping will be applied on the total energy if there is a nonzero stable branch φ^- in the solution, especially for large wavenumbers.

The typical evolutions of the flow solutions with strong resistivity $\alpha = 0.1$ and weak resistivity $\alpha = 5$ are compared in Figs. 2 and 3. First snapshot of the flow vorticity field $\zeta = \nabla^2 \varphi$ at the final computation time $t = 1000$ is compared with the initial configuration. The small value $\alpha = 0.1$ case drives the solution to a regime with only small-scale fluctuation vortices. The large-scale zonal structure from the initial state is not maintained and gets damped entirely at the final time. Then, the strong zonal particle transport is maintained. On the other hand with a large value $\alpha = 5$, the flow reaches closer to the one-field Hasegawa–Mima solution with a very rapidly decaying stable mode $\hat{\varphi}_k^- e^{-\alpha(1+k^{-2})t}$. The solution goes through the selective decay process and reaches a purely zonal flow structure with blocked turbulent flux transport. This clear transition from a non-zonal drift wave state ($\alpha = 0.1$) to the zonal flow dominant state ($\alpha = 5$) characterizes the typical Dimits shift [4,23] even in this limiting case of the BHW model.

To check in more details about the process of energy/enstrophy relocation in time, we also compute the ratio of enstrophy W_k/W and energy E_k/E at each scale measured at several different time instants during the evolution of the solution for the two test cases. Notice that the adiabaticity parameter α only adds isotropic effect to the system, so we focus on the energy in the nonzero fluctuation modes $k_y \neq 0$. By showing the normalized spectra, W_k/W and E_k/E, the different damping rates and energy transfer between scales can be characterized. With the small value $\alpha = 0.1$, clearly the fluctuation in enstrophy transports downscale to create more and more smaller-scale vortices until the hyperviscosity effect $\nu\Delta^s$ at the smallest scale takes over. This leads to more turbulent dynamics with stronger induced particle transport. In contrast with $\alpha = 5$, a weak downscale cascade only appears in the very beginning transient state (see $t = 100$ in Fig. 3b), and the fluctuation in enstrophy moves upscale finally in the other direction. In the normalized ratios, this shows the largest scales with small wavenumbers are dissipated at the slowest rate. This acts together with the formation of a strong zonal velocity state $\bar{v}$. Consistent with our previous analysis in (32), the zonal flow interaction with the particle flux will suppress the effect for forward energy cascade to smaller scales. Also, in the energy spectrum, the energy among E_k in large-scale modes is barely modified in time, while the strong dissipation is mostly applied on the small-scale modes. The strong dissipation at the small scales will finally drain the energy in small fluctuating vortices. This also illustrates the selective decay process from the dissipation operators.

3.3.2 Transition from drift wave turbulence to zonal flows

Next, we can also discover the transition from the drift wave dominant regime to the zonal flow dominant regime based on the limiting model (17). The abrupt transition from fully turbulent flow to a quiescent zonal flow state is usually known as Dimits shift and can be studies in the BHW model [23,25]. Here, we find that this limiting model $\kappa = 0$ is also able to recover the representative nonlinear transition by changing the values of α. In Fig. 4, we compare the typical converged flow states with three different values of $\alpha = 0.1, 0.5, 1$. Clearly we can observe the sharp transition in flow states with a homogeneous turbulent state with a small value of $\alpha = 0.1$, to regular zonal flow structure as α increases. This can be also seen from the opposite performance in the Dirichlet quotient $\Lambda = W/E$. An increase in Λ implies the forward energy cascade to create more small-scale turbulence, while a sharp drop in Λ below 1 infers the convergence to a purely zonal state.

We compare the time series of the total energy $E = \int |\nabla\varphi|^2 + n^2$ and the total enstrophy $W = \int q^2$ as well as the Dirichlet quotient Λ. The second row of Fig. 4 displays the results for the three typical parameter cases $\alpha = 0.1, 0.5, 1$. In this test with $\kappa = 0$, the total enstrophy W follows the dynamics (23) and is only subject to the dissipation effect. Therefore, we always observe the monotonic decreasing total enstrophy W in time for all three test cases. On the other hand, the total energy E follows the dynamical Eq. (30) with the particle resistivity due to α as well as the zonal flow interaction with $\bar{v}$ acting as a forcing effect. The solutions act differently for regime with a zonal state $\alpha = 1, 0.5$ and fully turbulent regime with a smaller $\alpha = 0.1$. In the turbulent regime with small α values, no zonal flow structure is formed; thus, the right hand side of (30) is still negative definite to induce decaying total energy E as in the $\alpha = 0.1$ case. However, zonal structures are developed as the value of α increases. Then, the zonal mean flow interaction term $\int \bar{v}\left(\widetilde{\tilde{u}\tilde{n}}\right)$

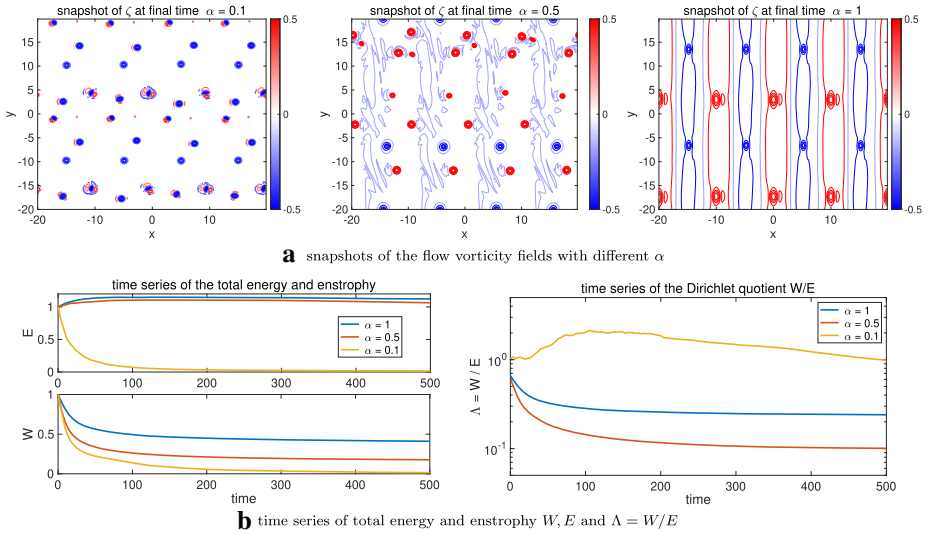

Fig. 4 Flow simulations with combined effects from different resistivity α and dissipation $\mu = 1 \times 10^{-4}$. The upper row shows the snapshots of the flow vorticity $\zeta = \nabla^2 \varphi$ at the final computation time; the lower row plots time series of the total energy E and enstrophy W as well as the ratio W/E with three different values of $\alpha = 0.1, 0.5, 1$

in the energy equation actually gives an important contribution to the full dynamics and drives the final energy to a higher level as in the $\alpha = 0.5, 1$ cases.

Further, we can track the evolution of the Dirichlet quotient $\Lambda = W/E$, especially for the convergence process. In the transient state, the energy first cascades downscale to generate more excited fluctuation modes (with an increase in the value of the ratio W/E) in the first stage with small values of α. This corresponds to the mechanism to create strong particle transport in the turbulence regime. After the transition to the zonal flow dominated regime, the flow solution directly decays to the stable zonal jet structure as the selective decay case with $\alpha = 0.5, 1$. Especially at the low resistivity limit $\alpha \to \infty$, the feedback from the stable branch $\hat{\varphi}^-$ vanishes and the model acts the same as the HM model selective decay process. These phenomena can be compared with the Dimits shift found in the general model case as in Fig. 3 and Fig. 7 in [25].

4 Extreme non-normal regime with zero adiabaticity $\alpha = 0$

In this section, we turn to the non-normal dynamics between the two aligned eigendirections. Here, from another perspective we focus on the other limiting regime at the hydrodynamical limit with $\alpha = 0$ while varying strength in background density gradient $\kappa \neq 0$. Unlike the previous limiting case in Sect. 3 with almost orthonormal eigenmodes, non-normal structures between the two eigendirections become important with $\kappa \neq 0$ as the parameter ratio $r = \kappa/\alpha$ increases. This becomes the typical regime to display extreme non-normal dynamics where the eigenvectors get aligned in the same direction (see Fig. 1 for the transition in non-normal structure between modes).

In this fully non-normal regime, there is again no linear instability injecting energy into the system. Therefore, it offers another clean setup for analyzing the reorganization of energy and enstrophy from different initial configurations in the transient state, especially

due to the particle flux and the effect from mean flow interaction. In the following part, we first discuss the model statistical solutions under the model non-normality; then, the extreme non-normal performance with $\alpha = 0$ is discussed in detail by comparing direct numerical simulation results.

4.1 Dynamical equations with two aligned eigendirections at the limit $\alpha = 0$

The BHW model (1) with zero adiabaticity $\alpha = 0$ for potential vorticity $q = \nabla^2\varphi - \tilde{n}$ and particle density n at the limit $\alpha = 0$ becomes

$$\begin{aligned} &\frac{\partial q}{\partial t} + \nabla^{\perp}\varphi \cdot \nabla q - \kappa \frac{\partial \varphi}{\partial y} = \mu \Delta q, \\ &\frac{\partial n}{\partial t} + \nabla^{\perp}\varphi \cdot \nabla n + \kappa \frac{\partial \varphi}{\partial y} = \mu \Delta n, \end{aligned} \tag{34}$$

In the limiting model above, the equation for density field n acts exactly as a tracer field with equivalent 'mean gradient' κ along x direction (see [19] for the corresponding tracer field formulation with a mean gradient) advected by the flow field generated by the electrostatic potential $\mathbf{v} = \nabla^{\perp}\varphi$. In the MHW model [2], the density field n becomes exactly passive without feedback to the flow equation for $\zeta = \nabla^2\varphi$. However, under the BHW model formulation, the density field inversely affects the flow structure through the zonal mean density profile $\overline{n}$. The auxiliary equation for the relative ion vorticity $\zeta = \nabla^2\varphi$ can be found as

$$\frac{\partial \zeta}{\partial t} + \nabla^{\perp}\varphi \cdot \nabla \zeta + \left[\tilde{u}\frac{\partial \overline{n}}{\partial x} - \frac{\partial}{\partial x}\left(\overline{\tilde{u}\tilde{n}}\right)\right] = \mu \Delta \zeta. \tag{35}$$

The zonal density $\overline{n}$ and the zonal particle flux $\overline{\tilde{u}\tilde{n}}$ can inversely give implicit feedback to the dynamics of the ion vorticity ζ. The above mean flow feedback also requires a nonzero velocity $\tilde{u}$. This provides an important difference in the BHW model that produces enhanced zonal jets and fluctuation modes interaction [23,24]. The limit at $\alpha = 0$ forms an effective extreme test case for the interacting mechanism of the zonal mean fields and fluctuating particle flux.

4.1.1 Non-normal eigenstates and the energetics

From the linear stability analysis (10), the two eigenvectors become aligned toward the same direction with the angle approaching zero $\theta_{\mathbf{k}} \to 0$ as the adiabaticity parameter $\alpha \to 0$. The growth rate for linear instability vanishes in the two same eigenvalues $\omega^{\pm} \equiv 0$ at the limit $\alpha = 0$. Correspondingly, the two eigenvectors get aligned together so that the two fluctuation modes have the same relation as follows:

$$\hat{q}_{\mathbf{k}} = -\hat{n}_{\mathbf{k}}, \quad \hat{\varphi}_{\mathbf{k}} \equiv 0, \tag{36}$$

with the corresponding decomposition for the potential vorticity and density state

$$\tilde{q} = \sum \hat{q}_{\mathbf{k}} e^{-\mu k^2 t} e^{i\mathbf{k}\cdot\mathbf{x}}, \ \tilde{n} = -\sum \hat{q}_{\mathbf{k}} e^{-\mu k^2 t} e^{i\mathbf{k}\cdot\mathbf{x}}. \tag{37}$$

If we only consider the non-zonal fluctuation modes $k_y \neq 0$, the non-normal state (36) gives the exact solution for the system (34) at $\alpha = 0$. On the other hand, small fluctuation in

the potential function φ together with the nonlinear interaction will lead to the formation of zonal jets. Then, the zonal density profile $\overline{n}$ will add an important feedback to the ion vorticity $\zeta = \nabla^2\varphi$ through the dynamics (35). Thus, the flow state is driven away from the aligned eigenvectors (37), and turbulence flow can be created.

The total enstrophy and energy Eq. (13) in the $\alpha = 0$ case are controlled by the total particle flux with the parameter κ. The dynamical equations for the total enstrophy W and total energy E then can be found as

$$\begin{aligned} W &= \int q^2, \quad \frac{\mathrm{d}W}{\mathrm{d}t} = \kappa \int \overline{\tilde{u}\tilde{n}} \; - \mu \int |\nabla q|^2, \\ E &= \int |\nabla\varphi|^2 + n^2, \quad \frac{\mathrm{d}E}{\mathrm{d}t} = \int (\kappa + \bar{v})\, \overline{\tilde{u}\tilde{n}} \; - \mu \int \left(|\Delta\varphi|^2 + |\nabla n|^2\right). \end{aligned} \tag{38}$$

For the effect of the parameter κ, it acts on the nonzero total particle flux $\int \overline{\tilde{u}\tilde{n}}$ from the initial state as a strong forcing on both energy and enstrophy dynamics. In fact, with modes only along the eigendirection with $\hat{q} = -\hat{n}$, the total enstrophy and energy become the same with zero contribution from the electrostatic potential $\varphi \equiv 0$

$$W = E = \sum |\hat{n}_{\mathbf{k}}|^2.$$

The difference between the total energy and enstrophy is then determined only from the zonal state feedbacks due to the advected flux term, $\int \bar{v}\left(\overline{\tilde{u}\tilde{n}}\right)$. Again this is the additional effect appearing only in the BHW model (see Section III in [14] for the MHW model case) that emphasizes the interactions with the zonal mean velocity. By taking the difference between the energy and enstrophy Eq. (38), we can find that the energy/enstrophy difference $E - W$ is only changed by the zonally advected particle flux through interaction with the zonal mean state $\bar{v}$ besides the dissipation effect

$$\frac{\mathrm{d}}{\mathrm{d}t}(E - W) = \int \bar{v}\left(\overline{\tilde{u}\tilde{n}}\right) \; - \mu \int \left(|\Delta\varphi|^2 + |\nabla n|^2 - |\nabla q|^2\right). \tag{39}$$

With a nonzero zonal mean flow $\bar{v}$, the advected flux will add another strong forcing on the total energy. We will illustrate these effect next from direct numerical simulations. To check the energy exchange mechanism, we can first track the time evolution of total enstrophy W for the effect from the total particle flux, $\kappa \int \overline{\tilde{u}\tilde{n}}$ and then track the time series of the difference $E - W$ for the effect from the advected flux, $\int \bar{v}\left(\overline{\tilde{u}\tilde{n}}\right)$.

4.1.2 Statistical steady-state solution starting from the aligned eigendirections

For the non-normal dynamics, we can find a set of exact solutions for the Eq. (34) with purely zonal electrostatic potential and the density field determined from its initial value

$$\varphi = \overline{\varphi}(x) = \sum_k \overline{\varphi}_k e^{-\mu k^2 t} e^{ikx}, \; u = -\partial_y\varphi \equiv 0, \quad n = \sum_{k_y \neq 0} \hat{n}_{\mathbf{k}}(0)\, e^{-\mu k^2 t} e^{i\mathbf{k}\cdot\mathbf{x}}. \tag{40}$$

This can be confirmed by directly putting the solutions (40) back into the original system (34). The solution is independent of the parameter κ. Since the system contains no linear instability, any perturbations $\tilde{\varphi}$ in the non-zonal flow field are effective through the nonlinear term with secondary instability [22]. In general from the previous analysis using secondary instability and selective decay [21,22], the non-zonal fluctuations will finally

get transferred back to the zonal modes and enforce the zonal state solution $\overline{\varphi}$. Thus, the above exact solution (40) is stable with the perturbations in the non-zonal fluctuations.

Next, we consider the balance between the statistical particle flux and the damping effects in the statistical steady state. From the enstrophy Eq. (38), a constant final statistical enstrophy requires the balance between the statistical particle flux and the damping effect

$$\left\langle \int \overline{\tilde{u}\tilde{n}} \right\rangle_{\text{eq}} = \frac{\mu}{\kappa} \left\langle |\nabla q|^2 \right\rangle_{\text{eq}} = \frac{\mu}{\kappa} \sum k^2 \left\langle |\hat{q}_{\mathbf{k}}|^2 \right\rangle_{\text{eq}}. \tag{41}$$

Above $\langle \cdot \rangle_{\text{eq}}$ refers to the statistical average in the statistical steady state (it can be viewed as the ensemble average among the simulation of a group of particles). Similarly, the statistical steady state of the energy requires the balance with the advected flux transport

$$\left\langle \int \overline{v} \left(\overline{\tilde{u}\tilde{n}} \right) \right\rangle_{\text{eq}} = \mu \int \left(\left\langle |\Delta \varphi|^2 \right\rangle_{\text{eq}} + \left\langle |\nabla n|^2 \right\rangle_{\text{eq}} - \left\langle |\nabla q|^2 \right\rangle_{\text{eq}} \right). \tag{42}$$

For the non-dissipative case $\mu = 0$, the a final steady statistical state requires the constraint in the flow advected fluxes, $\left\langle \int \overline{v} \left(\overline{\tilde{u}\tilde{n}} \right) \right\rangle_{\text{eq}} = 0$ and $\left\langle \int \overline{\tilde{u}\tilde{n}} \right\rangle_{\text{eq}} = 0$.

4.2 Statistical transition in flow solutions from direct numerical simulations

In this final section, we use direct numerical simulations to investigate the non-normal dynamics. We will mostly consider the non-normal interactions for the redistribution of energy and enstrophy in different scales (wavenumbers) in the starting transient process.

4.2.1 Transient statistics without dissipation effects

First, we focus on the contributions from the two nonlinear flux terms, $\kappa \int \overline{\tilde{u}\tilde{n}}$ and $\int \overline{v} \left(\overline{\tilde{u}\tilde{n}} \right)$, without the inclusion of dissipation effect $\mu = 0$. In this way, the nonlinear exchanges of energy and enstrophy along scales in the dynamics (38) and (39) purely due to fluctuation interaction with and without a zonal mean flow $\overline{v}$ from the starting transient state can be compared. To compare the performance with different zonal mean profiles $\overline{v}$, we pick the same two typical initial states used in the previous test cases in Figs. 2 and 3, which are also plotted in Fig. 5. The first case (left) generates more homogeneous turbulence with only a weak zonal flow, while the second case (left) gives a strong zonal state $\overline{v}$ from the initial setup. The numerical setup of the model is the same as described in Sect. 3.3. We then track their evolutions in the transient stage departing from the two different initial configurations.

In Fig. 6, we first plot the time series of the total enstrophy W subject to the total particle flux $\kappa \int \overline{\tilde{u}\tilde{n}}$, and the difference $E - W$ subject to the advected flux $\int \overline{v} \left(\overline{\tilde{u}\tilde{n}} \right)$. Two different initial states in Fig. 5 with and without a dominant zonal jets $\overline{v}$ are compared. And no dissipation $\mu = 0$ is introduced in this test to identify the particular nonlinear flux effect. Thus, we can focus on the nonlinear coupling from the two flux terms during the transient evolution of the system. First in the time series of the total enstrophy, the solution is subject to the total particle flux according to (38). The nonzero zonal flow excites strong particle flux and raises the enstrophy to a much higher level from the starting initial state. In contrast, the enstrophy from the case without a dominant zonal flow just decays in time even though it starts with a larger value of the particle flux. The effect of the zonal mean

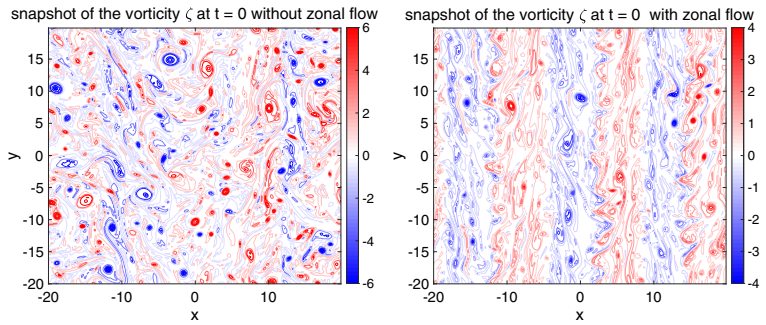

Fig. 5 Two initial states of the ion vorticity without (left) and with (right) a dominant zonal mean flow $\bar{v}$ for the simulations with $\alpha = 0$

flow can be observed more clearly in the time series of the energy and enstrophy difference $E - W$. With a nonzero mean flow, a strong advected flux $\int \bar{v}\left(\widetilde{\tilde{u}\tilde{n}}\right)$ in the dynamics (39) is induced in the starting time, greatly raising the level of total energy. In particular, this effect from the zonal mean state $\bar{v}$ is only modeled in the BHW model [14,24]. This will lead to the more turbulent zonal jets with larger variability as observed in the previous BHW simulations (see Fig. 3 and Fig. 4 in [24] for a comparison with the MHW model results).

To check in more details about the energy and enstrophy exchanges in different scales, the second and third rows of Fig. 6 compare the enstrophy and energy spectra in fluctuation modes $k_y \neq 0$ with the two different initial states measured at several typical time instants. With a nonzero initial zonal mean state $\bar{v}$ (second row of Fig. 6), energy among several larger/intermediate scales first gets excited due to the strong nonlinear flux impulse in $\kappa \int \widetilde{\tilde{u}\tilde{n}}$ and $\int \bar{v}\left(\widetilde{\tilde{u}\tilde{n}}\right)$. The enstrophy then quickly cascades downscales and gets dissipated by the hyperviscosity at the smallest scale mode. In comparison, the energy goes inversely upscale to create a dominant most energetic large-scale mode. In the case with a dominant zonal mean state (second row of Fig. 6), again only decaying energy and enstrophy spectra are shown from the initial configuration. Without the contribution from a strong zonal flow $\bar{v}$, the nonlinear flux is not strong enough to excite the fluctuation modes. The energy and enstrophy effectively move all the way downscale to smallest resolved scale to get fast dissipated by the hyperviscosity. This leads to the entire quench of zonal particle transport.

The typical flow vorticity snapshots in the starting transient states with nonzero zonal jet $\bar{v}$ are plotted in Fig. 7 to illustrate the detailed flow transition in time. It can be seen that the initial multiple jet structure gets distorted in time and finally reach the steady zonal structure in the largest scale zonal state. More energy gets moved to the larger scales, and the turbulent transport finally gets reduced to the minimum. Finally, the flow approaches the purely zonal structure with all the non-zonal fluctuation modes dissipated to zero. We see the relocation of energy in different scales due to the drift wave effect from the model parameter κ.

4.2.2 Flow transition in statistics with different values of the density gradient κ

Next, we consider the effect from different values of the background density gradient κ. In this test case, we compare the transition in flow structures in the final statistical steady

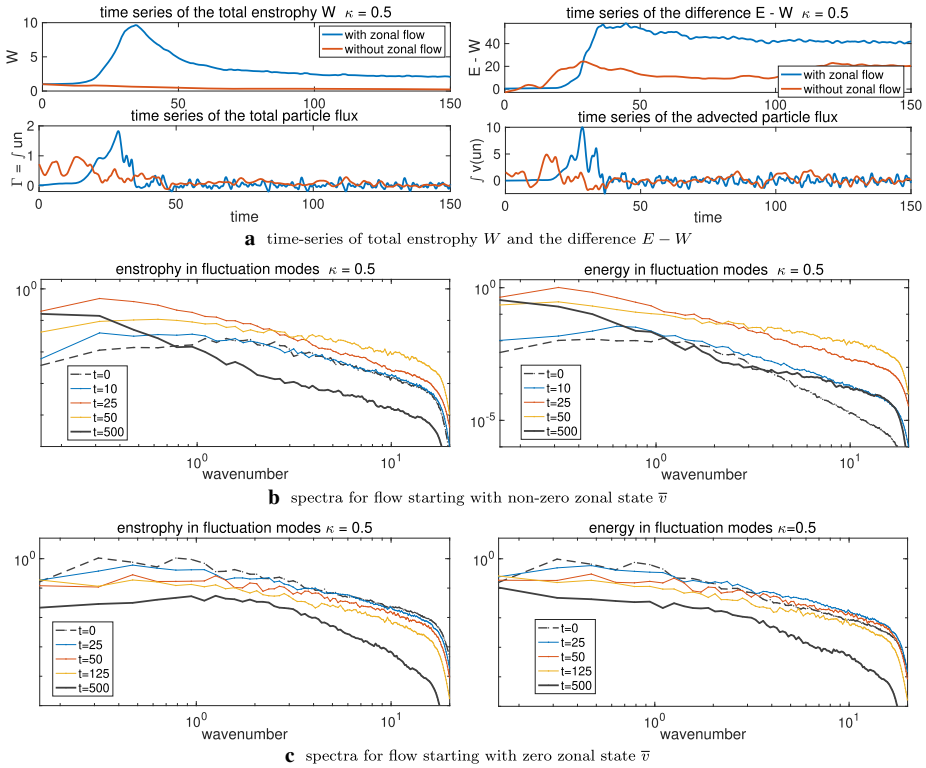

Fig. 6 Evolution of energy and enstrophy in the limiting regime $\alpha = 0, \kappa = 0.5$ without dissipation effect $\mu = 0$. Upper row: time series of the total enstrophy W and the difference between energy and enstrophy $E - W$, as well as the particle flux and advected flux, $\int \bar{u}\bar{n}$ and $\int \bar{v}\left(\bar{u}\bar{n}\right)$ as forcing effects. Lower rows: enstrophy and energy spectra in fluctuation modes measured at several different time instants. The initial spectra are plotted with dashed black lines, and the spectra at final time are shown in solid black. Two different initial states with and without an zonal velocity $\bar{v}$ are compared

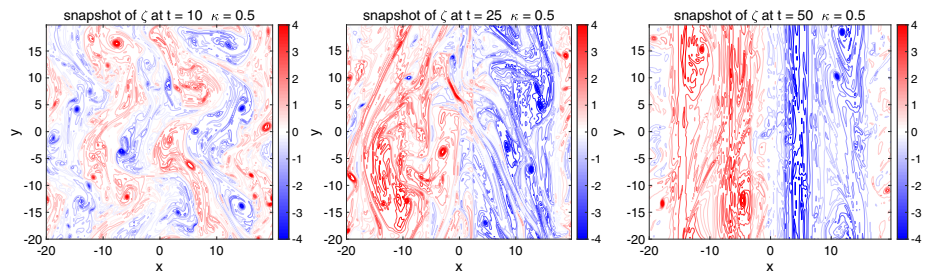

Fig. 7 Flow vorticity $\zeta = \nabla^2\varphi$ snapshots at the transient time instants starting from the initial state with a nonzero zonal velocity $\bar{v}$ without dissipation effect $\mu = 0$

states. The same small homogeneous dissipation $\mu = 1 \times 10^{-4}$ as in Sect. 3 is added with three typical values of the parameter $\kappa = 0.05, 0.5, 5$. As $\kappa \to 0$ goes to small values, there is a smaller weight added on the total particle flux, $\kappa \int \bar{u}\bar{n}$, in both the total energy and enstrophy Eq. (38). With large values of κ, on the other hand, much stronger flux forcing is exerted to increase the amplitudes of total energy and enstrophy.

Figure 8 shows the final steady states of the ion vorticity snapshots and statistics in energy and enstrophy spectra. With small values of κ, the solution converges closer to the case as the one-layer barotropic system [17]. The flow goes through the selective

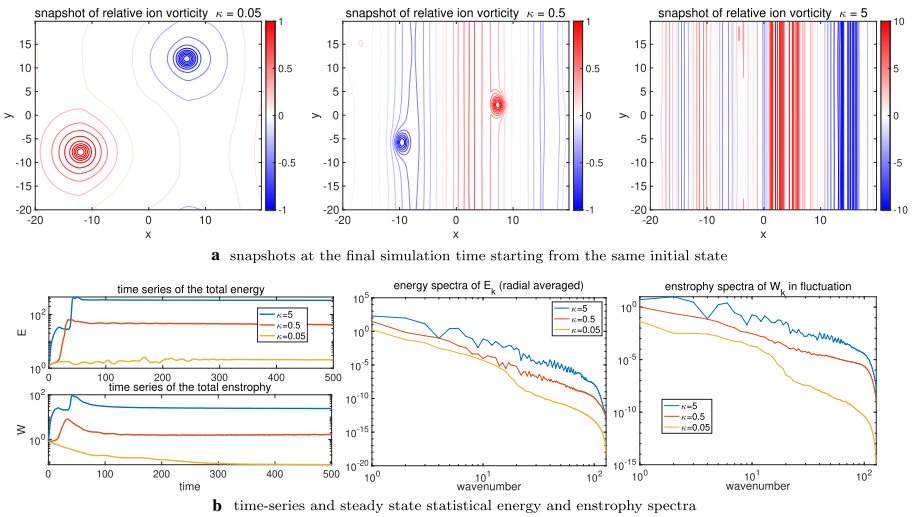

Fig. 8 Comparison of the final state flow ion vorticity $\zeta = \nabla^2\varphi$ snapshots (upper row) and time series and steady-state statistical spectra in energy and enstrophy (lower row) with three different values of $\kappa = 0.05, 0.5, 5$. The initial state is taken the same with a nonzero zonal flow, and small dissipation $\mu = 1 \times 10^{-4}$ with $\alpha = 0$ is used

decay process to the homogeneous largest scale [21]. As the value of κ increases, the flow becomes more energetic due to the impulsive forcing from the particle flux, $\kappa \int \tilde{u}\tilde{n}$ in the transient state. Within this $\alpha = 0$ regime, since there is no linear instability, the energy gets redistributed between scales in the transient state and will finally go to the zonal modes through the selective decay and secondary instability energy transfer. Then, through the nonlinear secondary transfer of energy [21], the energy finally all gets converted to the zonal state as in the large value κ case.

Finally, the second row of Fig. 8 compares the time series of total energy and enstrophy in time with different values of κ and $\alpha = 0$. Larger value of κ induces a higher saturated level of total energy and enstrophy in the final statistical steady state. This is purely from the non-normal dynamics without linear instability at the extreme limiting case with $\alpha = 0$. By comparing the final statistical energy and enstrophy spectra, larger values of κ generate more energetic energy/enstrophy among all scale modes. With a small value of κ, the nonzero particle flux has little effect on the total energy and enstrophy. The system goes through the selective decay to leave only the largest scales.

5 Summary

To summarize, we studied two limiting dynamical regimes of the magnetically confined plasma system for the analysis of nonlinear interactions in turbulent drift waves and zonal flow in plasma edge turbulence. The flux-balanced Hasegawa–Wakatani (BHW) model [14] is taken as the base model to characterize the representative structures in a simplified two-field formulation. Especially, the limiting regimes separate the contributions from the non-adiabatic resistivity α and the background density gradient κ in the BHW model to be studied individually. The two-field model can be decomposed into a group of 2×2 subsystems by projecting the corresponding linearized equation onto two characteristic eigendirections. The system displays a continuous transition from completely decou-

pled subsystems with orthonormal eigendirections to the extreme non-normal dynamics according to the ratio κ/α of the two model parameters. The extreme dynamics according to the eigenvalue decomposition then can be categorized into two representative limiting regimes. New *a priori* estimates are developed for the two limiting regimes as basic guidelines for characterizing the effects from various physical processes modeled in the two-field BHW framework. The conclusions are derived from heuristic mathematical argument and are confirmed by direct numerical simulations.

The first limiting regime assumes zero background density gradient $\kappa = 0$ and varies the adiabaticity parameter α. The total energy and enstrophy equation predict a conserved enstrophy with decaying energy in time. The special energetics structure implies that we can apply the strategies in selective decay theory used in the one-field model previously [21] to this more complicated two-field limiting case. To predict the dual direction of nonlinear energy transfer between scales, we track the time evolution of the Dirichlet quotient Λ as an index to measure the rate of energy exchange among different scales. The competing effects from the model dissipation, non-adiabatic particle resistivity, and the nonlinear interaction with a zonal flow can be identified based on the framework. The theoretical implications are further confirmed with direct numerical simulations of the BHW model. From the other limiting regime with zero adiabaticity $\alpha = 0$, we are able to check the effect from extreme non-normal dynamics with two aligned eigendirections. This case gives a density field advected by turbulent magnetic flow similar to the passive tracer advection model with a mean gradient investigated in [19]. A typical statistical transition from homogenous turbulence to the generation of regularized zonal jets is also recovered in this extreme limiting regime and is again illustrated by extensive numerical simulations. The promising results in the two limiting regimes in this paper support the potential of the BHW model to better characterize the various representative features in particular plasma edge regimes such as the Dimits shift and avalanche-like structures [23,25] under a simplified model framework.

Acknowledgements
This research of A.J.M. is partially supported by the Office of Naval Research N00014-19-1-2286. D.Q. is supported as a postdoctoral fellow on the Grant. On behalf of both authors, the corresponding author states that there is no conflict of interest.

A The most likely state of the two-field BHW model from the variational principle

The physicists' selective decay principle [15] states that the long time behavior of the system reaches the states with minimized energy in a given constant energy. However, from the enstrophy and energy Eqs. (23) and (24) for the limiting model $\kappa = 0$ implies that the energy will decay in a much faster rate compared with a relatively constant enstrophy in the case with a dominant adiabaticity factor α. For both cases, the selective decay state can be discovered by computing the critical solution under the variational principle. Here, we propose to compute the selective decay states directly through the Lagrangian multiplier method. This may offer us some intuition about the structures in the group of admissible solutions. The strategy is generalized from the basic variational method approach detailed in Section 4 of [21] for the one-field HM model.

Directly from the definition (12), the total energy and enstrophy for the BHW model can be found as

$$E(\varphi, n) = \frac{1}{2}\int \left(|\nabla\varphi|^2 + n^2\right),$$
$$W(\varphi, \tilde{n}) = \frac{1}{2}\int (\Delta\varphi - \tilde{n})^2.$$

In the two-field BHW model, energy and enstrophy should be determined by both electrostatic potential φ and density fluctuation n. The variational principle here is to find the extrema of the energy E given a constant enstrophy W. According to the Lagrangian multiplier method, we need to solve the following variational relations with Γ as the Lagrangian multiplier

$$\begin{aligned} \frac{\delta E}{\delta\varphi} &= \Gamma\frac{\delta W}{\delta\varphi}, \\ \frac{\delta E}{\delta\tilde{n}} &= \Gamma\frac{\delta W}{\delta\tilde{n}}. \end{aligned} \tag{A.1}$$

The variational derivatives for the quadratic functionals W and E can be first computed directly as

$$\frac{\delta W}{\delta\varphi} = \left(\Delta^2\varphi - \Delta\tilde{n}\right), \quad \frac{\delta W}{\delta\tilde{n}} = -\left(\Delta\varphi - \tilde{n}\right),$$
$$\frac{\delta E}{\delta\varphi} = -\Delta\varphi, \quad \frac{\delta E}{\delta\tilde{n}} = \tilde{n}.$$

Substituting the above derivatives back to the Euler–Lagrangian equations (A.1), we find the critical state solution $(\bar{\varphi}^*, \tilde{\varphi}^*, \tilde{n}^*)$ in the following relations:

$$\begin{aligned} \partial_x^2\bar{\varphi}^* &= -\Gamma\partial_x^4\bar{\varphi}^* = 0, \\ \Delta\tilde{\varphi}^* &= -\Gamma\Delta\left(\Delta\tilde{\varphi}^* - \tilde{n}^*\right), \\ \tilde{n}^* &= -\Gamma\left(\Delta\tilde{\varphi}^* - \tilde{n}^*\right). \end{aligned}$$

For convenience, we separate the zonal and fluctuation components in the state variables. The first equation above for the zonal state implies a constant zonal velocity $\bar{v} = V_0 =$ const. Notice that the additional constant zonal profile will not alter the solution structure since the BHW model is Galilean invariant [24]. Then, the critical solution goes to a purely fluctuation state satisfying

$$\begin{aligned} \Delta\tilde{\varphi}^* &= \Delta\tilde{n}^*, \\ \Delta^2\tilde{\varphi}^* &= \left(1 - \Gamma^{-1}\right)\Delta\tilde{\varphi}^*. \end{aligned} \tag{A.2}$$

This gives the HM state (18) with the density fluctuation converging to the electrostatic potential in a single constant wavenumber $k = |\mathbf{k}|$

$$\tilde{\varphi}^* = \tilde{n}^* = \sum_{k^2=\Gamma^{-1}-1} \hat{\varphi}_{\mathbf{k}}^+ e^{i\mathbf{k}\cdot\mathbf{x}}, \tag{A.3}$$

and the permitted Lagrangian multiplier $\Gamma < 1$. The critical exact solution also implies the corresponding Dirichlet quotient (25)

$$\Lambda = \frac{W}{E} = \Gamma^{-1}.$$

Combined with the monotonically decreasing Λ due to the resistivity effect (29), we see the solution is driven to the critical point (A.3) with the minimum permitted value of

Γ. The final permitted selective decay state is the single-mode solution with the largest resolved wavenumber. The variational principle predicts the same smallest scale state from the reversed selective decay due to the particle resistivity.

Received: 14 April 2020 Accepted: 3 July 2020 Published online: 21 July 2020

References

1. Balescu, R.: Aspects of Anomalous Transport in Plasmas. CRC Press, Cambridge (2005)
2. Dewar, R.L., Abdullatif, R.F.: Zonal flowgeneration bymodulational instability. In: Denier J., Frederiksen J.S. (eds.) Frontiers in Turbulence and Coherent Structures. Proceedings of the COSNet/CSIRO Workshop on Turbulence and Coherent Structures in Fluids, Plasmas and Nonlinear Media, The Australian National University, Canberra, Australia, 10–13 January 2006. World Scientific. https://doi.org/10.1142/6320
3. Diamond, P.H., Itoh, S., Itoh, K., Hahm, T.: Zonal flows in plasma—a review. Plasma Phys. Control. Fus. **47**(5), R35 (2005)
4. Dimits, A.M., Bateman, G., Beer, M., Cohen, B., Dorland, W., Hammett, G., Kim, C., Kinsey, J., Kotschenreuther, M., Kritz, A., et al.: Comparisons and physics basis of tokamak transport models and turbulence simulations. Phys. Plasmas **7**(3), 969–983 (2000)
5. Dorland, W., Hammett, G.: Gyrofluid turbulence models with kinetic effects. Phys. Fluids B Plasma Phys. **5**(3), 812–835 (1993)
6. Hasegawa, A., Mima, K.: Pseudo-three-dimensional turbulence in magnetized nonuniform plasma. Phys. Fluids **21**(1), 87–92 (1978)
7. Hasegawa, A., Wakatani, M.: Plasma edge turbulence. Phys. Rev. Lett. **50**(9), 682 (1983)
8. Horton, W.: Drift waves and transport. Rev. Mod. Phys. **71**, 735–778 (1999). https://doi.org/10.1103/RevModPhys.71.735
9. Majda, A.J.: Introduction to Turbulent Dynamical Systems in Complex Systems. Springer, Berlin (2016)
10. Majda, A.J., Holen, M.: Dissipation, topography, and statistical theories for large-scale coherent structure. Commun. Pure Appl. Math. A J. Issued Courant Inst. Math. Sci. **50**(12), 1183–1234 (1997)
11. Majda, A.J., Qi, D.: Strategies for reduced-order models for predicting the statistical responses and uncertainty quantification in complex turbulent dynamical systems. SIAM Rev. **60**(3), 491–549 (2018)
12. Majda, A.J., Qi, D.: Linear and nonlinear statistical response theories with prototype applications to sensitivity analysis and statistical control of complex turbulent dynamical systems. Chaos Interdiscip. J. Nonlinear Sci. **29**(10), 103131 (2019)
13. Majda, A.J., Qi, D.: Statistical phase transitions and extreme events in shallow water waves with an abrupt depth change. J. Stat. Phys. 179, 1718–1741 (2020). https://doi.org/10.1007/s10955-019-02465-3
14. Majda, A.J., Qi, D., Cerfon, A.J.: A flux-balanced fluid model for collisional plasma edge turbulence: model derivation and basic physical features. Phys. Plasmas **25**(10), 102307 (2018)
15. Majda, A.J., Shim, S.Y., Wang, X.: Selective decay for geophysical flows. Methods Appl. Anal. **7**(3), 511–554 (2000)
16. Majda, A.J., Tong, X.T.: Intermittency in turbulent diffusion models with a mean gradient. Nonlinearity **28**(11), 4171 (2015)
17. Majda, A.J., Wang, X.: Nonlinear Dynamics and Statistical Theories for Basic Geophysical Flows. Cambridge University Press, Cambridge (2006)
18. Numata, R., Ball, R., Dewar, R.L.: Bifurcation in electrostatic resistive drift wave turbulence. Phys. Plasmas **14**(10), 102312 (2007)
19. Qi, D., Majda, A.J.: Predicting fat-tailed intermittent probability distributions in passive scalar turbulence with imperfect models through empirical information theory. Commun. Math. Sci. **14**(6), 1687–1722 (2016)
20. Qi, D., Majda, A.J.: Linking the two-field dynamics of plasma edge turbulence with the one-field balanced model through systematic unstable forcing at low resistivity. Phys. Plasmas **26**(5), 052108 (2019)
21. Qi, D., Majda, A.J.: Transient metastability and selective decay for the coherent zonal structures in plasma drift wave turbulence. J. Nonlinear Sci. **29**(5), 2297–2339 (2019)
22. Qi, D., Majda, A.J.: Zonal jet creation from secondary instability of drift waves for plasma edge turbulence. Chin. Ann. Math. Ser. B **40**(6), 869–890 (2019)
23. Qi, D., Majda, A.J.: Flux-balanced two-field plasma edge turbulence in a channel geometry. Phys. Plasmas **27**(3), 032304 (2020)
24. Qi, D., Majda, A.J., Cerfon, A.J.: A flux-balanced fluid model for collisional plasma edge turbulence: numerical simulations with different aspect ratios. Phys. Plasmas **26**(8), 082303 (2019)
25. Qi, D., Majda, A.J., Cerfon, A.J.: Dimits shift, avalanche-like bursts, and solitary propagating structures in the two-field flux-balanced Hasegawa-Wakatani model for plasma edge turbulence. Submitted to Phys. Plasmas. arXiv preprint arXiv:2006.10554 (2020)
26. St-Onge, D. (2017). On non-local energy transfer via zonal flow in the Dimits shift. J. Plasma Phys. 83(5), 905830504. https://doi.org/10.1017/S0022377817000708
27. Wakatani, M., Hasegawa, A.: A collisional drift wave description of plasma edge turbulence. Phys. Fluids **27**(3), 611–618 (1984)
28. Zhu, H., Zhou, Y., Dodin, I.: Theory of the tertiary instability and the Dimits shift from reduced drift-wave models. Phys. Rev. Lett. **124**(5), 055002 (2020)

Publisher's Note